

SPATIALLY QUASI-PERIODIC WATER WAVES OF INFINITE DEPTH

JON WILKENING AND XINYU ZHAO

ABSTRACT. We formulate the two-dimensional gravity-capillary water wave equations in a spatially quasi-periodic setting and present a numerical study of solutions of the initial value problem. We adopt a conformal mapping formulation and employ a quasi-periodic version of the Hilbert transform to determine the normal velocity of the free surface. Four methods of time-stepping the initial value problem are proposed, two explicit Runge-Kutta (ERK) methods and two exponential time-differencing (ETD) schemes. The ETD approach makes use of the small-scale decomposition to eliminate stiffness due to surface tension. We perform a convergence study to compare the accuracy and efficiency of the methods on a traveling wave test problem. We also present an example of a periodic wave profile containing vertical tangent lines that is set in motion with a quasi-periodic velocity potential. As time evolves, some of the waves overturn while others flatten out. Beyond water waves, we argue that spatial quasi-periodicity is a natural setting to study the dynamics of linear and nonlinear waves, offering a third option to the usual modeling assumption that solutions either evolve on a periodic domain or decay at infinity.

1. INTRODUCTION

Linear and nonlinear wave equations are generally studied under the assumption that the solution is spatially periodic or decays to zero at infinity [25]. Beginning with Berenger [6], a great deal of effort has been devoted to developing perfectly matched layer (PML) techniques for imposing absorbing boundary conditions over a finite computational domain to simulate wave propagation problems on unbounded domains. However, in many situations, assuming the waves decay to zero at infinity is not a realistic model. For example, a large body of water such as the ocean is often covered in surface waves in every direction over vast distances. But assuming spatial periodicity may limit one's ability to observe interesting dynamics. In this paper, we formulate the initial value problem of the surface water wave equations in a spatially quasi-periodic setting, design numerical algorithms to compute such waves, and study their properties. We consider only the case of a two-dimensional fluid and limit our numerical computations to waves with two spatial quasi-periods.

One motivation for studying water waves in a quasi-periodic setting is that integrable model equations such as the Korteweg-de Vries equation and the Benjamin-Ono equation possess infinite hierarchies of quasi-periodic solutions [15, 19]. It is therefore natural to seek analogues for the free-surface Euler equations. Of course, periodic traveling water waves [18, 28, 34] and standing water waves [31–33, 38] are well-known, and have been an active topic of research for more than a century. But quasi-periodic dynamics of water waves have only been considered recently. Berti *et al* [5, 8] have proved the existence

This work was supported in part by the National Science Foundation under award number DMS-1716560 and by the Department of Energy, Office of Science, Applied Scientific Computing Research, under award number DE-AC02-05CH11231.

of small-amplitude temporally quasi-periodic gravity-capillary waves using Nash-Moser theory. Relative-periodic [39] and traveling-standing [40] water wave solutions have been computed by Wilkening; however, as with [5, 8], these solutions are quasi-periodic in time rather than space.

Subharmonic stability studies [14, 27, 35, 40] of periodic traveling and standing water waves point to unstable perturbation directions with wavelengths that are incommensurate with that of the underlying wave. This calls for the development of methods to explore the dynamics of such perturbations beyond linearization. Another motivation for studying spatially quasi-periodic water waves is the work of Wilton [42], who observed that a resonance can occur that causes Stokes' regular perturbation expansion for traveling water waves to break down [2, 35, 36]. Suppose k_1 and k_2 are both roots of the dispersion relation for linearized water waves of infinite depth,

$$(1.1) \quad c^2 = gk^{-1} + \tau k,$$

and $k_2 = Kk_1$ with $K \geq 2$ an integer. Then the K th harmonic will enter a modified Stokes expansion for traveling waves of wavelength $2\pi/k_1$ at order $\varepsilon^{\max(K-2,1)}$ instead of ε^K , where ε is the expansion coefficient of the fundamental mode. This resonance occurs because the two waves travel at the same speed under the linearized water wave equations. Bridges and Dias [9] consider a generalization in which the wave numbers k_1 and k_2 are irrationally related. They use a spatial Hamiltonian structure to construct weakly nonlinear approximations of spatially quasi-periodic traveling gravity-capillary waves for two special cases: deep water and shallow water. This inspired us to develop a framework for computing spatially quasi-periodic, fully nonlinear traveling gravity-capillary waves, which is the topic of the companion paper [41].

The present paper focuses on the more general spatially quasi-periodic initial value problem, which we use to validate the traveling wave computations and explore new dynamic phenomena. We use a conformal mapping formulation [11, 17, 26] of the gravity-capillary water wave problem, which differs from the approach in [9]. In particular, we introduce a Hilbert transform for quasi-periodic functions to compute the normal velocity and maintain a conformal parametrization of the free surface. This leads us to a numerical method to compute the time evolution of solutions of the Euler equations from arbitrary quasi-periodic initial data. We present two variants of the method, one in a high-order explicit Runge-Kutta framework and one in an exponential time-differencing framework. The former is suitable for the case of zero or small surface tension while the latter makes use of the small-scale decomposition [22, 23] to eliminate stiffness due to surface tension. We present a convergence study of the methods as well as a large-scale computation of a quasi-periodic wave in which some of the wave crests overturn when evolved forward in time while others flatten out. The computation involves over 33 million degrees of freedom evolved over 5400 time steps to maintain double-precision accuracy.

We include two appendices that cover various technical aspects of spatially quasi-periodic water waves that arose in the course of this work. In Appendix A, we prove a theorem establishing sufficient conditions for an analytic function $z(w)$ to map the lower half-plane topologically onto a semi-infinite region bounded above by a parametrized curve and for $1/|z_w|$ to be uniformly bounded. In Appendix B, we study families of quasi-periodic solutions obtained by introducing phases in the reconstruction formula for extracting 1d quasi-periodic functions from periodic functions on a torus. This enables us to prove that

if all the solutions in the family are single-valued and have no vertical tangent lines, the solutions are also quasi-periodic in the original graph-based formulation of the Euler equations. We also present a simple procedure for computing the change of variables from the conformal representation to the graph representation.

2. MATHEMATICAL FORMULATION

In this section, we review the governing equations for gravity-capillary waves in physical space and their conformal mapping formulation. We then extend the formulation to allow for spatially quasi-periodic solutions. For simplicity, we initially assume the wave profile $\eta(x, t)$ remains single-valued. This assumption is relaxed when discussing the conformal formulation, and an example of a wave in which some of the peaks overturn as time advances is presented in Section 4.2.

2.1. Governing Equations in Physical Space. Gravity-capillary waves of infinite depth are governed by the two-dimensional free-surface Euler equations [13, 43]

$$(2.1) \quad \eta(x, 0) = \eta_0(x), \quad \varphi(x, 0) = \varphi_0(x), \quad t = 0,$$

$$(2.2) \quad \begin{aligned} \Phi_{xx} + \Phi_{yy} &= 0, & -\infty < y < \eta(x, t), \\ \Phi_y &\rightarrow 0, & y \rightarrow -\infty, \\ \Phi &= \varphi, & y = \eta(x, t), \end{aligned}$$

$$(2.3) \quad \eta_t = \Phi_y - \eta_x \Phi_x, \quad y = \eta(x, t),$$

$$(2.4) \quad \varphi_t = \Phi_y \eta_t - \frac{1}{2} \Phi_x^2 - \frac{1}{2} \Phi_y^2 - g\eta + \tau \frac{\eta_{xx}}{(1 + \eta_x^2)^{3/2}} + C(t), \quad y = \eta(x, t),$$

where x is the horizontal coordinate, y is the vertical coordinate, t is the time, $\Phi(x, y, t)$ is the velocity potential, $\eta(x, t)$ is the free surface elevation,

$$(2.5) \quad \varphi(x, t) = \Phi(x, \eta(x, t), t)$$

is the boundary value of the velocity potential on the free surface, g is the vertical acceleration due to gravity and τ is the coefficient of surface tension. The function $C(t)$ in the Bernoulli condition (2.4) is an arbitrary integration constant that is allowed to depend on time but not space. We generally choose $C(t)$ so that the mean value of $\varphi(x, t)$ remains constant in time.

2.2. The Quasi-Periodic Hilbert Transform. We find that a conformal mapping representation of the free surface greatly simplifies the solution of the Laplace equation for the velocity potential in the quasi-periodic setting. In this section, we establish the properties of the Hilbert transform that will be needed to study quasi-periodic water waves in a conformal mapping framework.

A quasi-periodic, real analytic function $u(\alpha)$ is a function of the form

$$(2.6) \quad u(\alpha) = \tilde{u}(\mathbf{k}\alpha), \quad \tilde{u}(\boldsymbol{\alpha}) = \sum_{\mathbf{j} \in \mathbb{Z}^d} \hat{u}_{\mathbf{j}} e^{i\langle \mathbf{j}, \boldsymbol{\alpha} \rangle}, \quad \alpha \in \mathbb{R}, \quad \boldsymbol{\alpha}, \mathbf{k} \in \mathbb{R}^d,$$

where $\langle \cdot, \cdot \rangle$ denotes the standard inner product in \mathbb{R}^d and \tilde{u} is a periodic, real analytic function defined on the n -dimensional torus

$$(2.7) \quad \mathbb{T}^d := [0, 2\pi)^d.$$

Entries of the vector \mathbf{k} are required to be linearly independent over \mathbb{Z} . Since \tilde{u} is real-valued, $\hat{u}_{-j} = \overline{\hat{u}_j}$. Analyticity is equivalent to the requirement that there exist positive numbers M and σ such that $|\hat{u}_j| \leq M e^{-\sigma|j|}$, i.e. that the Fourier modes \hat{u}_j decay exponentially as $|j| \rightarrow \infty$. We define projection operators P and P_0 that act on u and \tilde{u} via

$$(2.8) \quad P = \text{id} - P_0, \quad P_0[u] = P_0[\tilde{u}] = \hat{u}_0 = \frac{1}{(2\pi)^d} \int_{\mathbb{T}^d} \tilde{u}(\boldsymbol{\alpha}) d\alpha_1 \dots d\alpha_d.$$

Note that P projects onto the space of zero-mean functions while P_0 returns the mean value, viewed as a constant function on \mathbb{R} or \mathbb{T}^d .

Given $u(\alpha)$ as above, the most general bounded analytic function $f(w)$ in the lower half-plane whose real part agrees with u on the real axis has the form

$$(2.9) \quad f(w) = \hat{u}_0 + i\hat{v}_0 + \sum_{\langle \mathbf{j}, \mathbf{k} \rangle < 0} 2\hat{u}_j e^{i\langle \mathbf{j}, \mathbf{k} \rangle w}, \quad (w = \alpha + i\beta, \beta \leq 0)$$

where $\hat{v}_0 \in \mathbb{R}$ and the sum is over all $\mathbf{j} \in \mathbb{Z}^d$ satisfying $\langle \mathbf{j}, \mathbf{k} \rangle < 0$. The imaginary part of $f(z)$ on the real axis is given by

$$(2.10) \quad v(\alpha) = \tilde{v}(\mathbf{k}\alpha), \quad \tilde{v}(\boldsymbol{\alpha}) = \sum_{\mathbf{j} \in \mathbb{Z}^d} \hat{v}_j e^{i\langle \mathbf{j}, \boldsymbol{\alpha} \rangle}, \quad \hat{v}_j = i \operatorname{sgn}(\langle \mathbf{j}, \mathbf{k} \rangle) \hat{u}_j, \quad (\mathbf{j} \neq 0)$$

where $\operatorname{sgn}(q) \in \{1, 0, -1\}$ depending on whether $q > 0$, $q = 0$ or $q < 0$, respectively. Similarly, given $v(\alpha)$ and requiring $(\operatorname{Im} f)|_{\mathbb{R}} = v$ yields (2.9) with \hat{u}_j replaced by $i\hat{v}_j$. We introduce a quasi-periodic Hilbert transform to compute v from u or u from v ,

$$(2.11) \quad v = \hat{v}_0 - H[u], \quad u = \hat{u}_0 + H[v],$$

where the constant $\hat{v}_0 = P_0[v]$ or $\hat{u}_0 = P_0[u]$ is a free parameter when computing v or u , respectively. H returns the “zero-mean” solution, i.e. $P_0 H[u] = 0$. Uniqueness of the bounded extension from u or v to f up to the additive constant $i\hat{v}_0$ or \hat{u}_0 follows from two well-known results: the only bounded solution of the Laplace equation on a half-space satisfying homogeneous Dirichlet boundary conditions is identically zero [4], and the harmonic conjugate of the zero function on a connected domain is constant.

Definition 2.1. The Hilbert transform of a quasi-periodic, analytic function $u(\alpha)$ of the form (2.6) is defined to be

$$(2.12) \quad H[u](\alpha) = \sum_{\mathbf{j} \in \mathbb{Z}^d} (-i) \operatorname{sgn}(\langle \mathbf{j}, \mathbf{k} \rangle) \hat{u}_j e^{i\langle \mathbf{j}, \mathbf{k} \rangle \alpha}.$$

This agrees with the standard definition [18] of the Hilbert transform as a Cauchy principal value integral:

$$(2.13) \quad H[u](\alpha) = \frac{1}{\pi} \operatorname{PV} \int_{-\infty}^{\infty} \frac{u(\xi)}{\alpha - \xi} d\xi.$$

Indeed, it is easy to show that for functions of the form $u(\alpha) = e^{i\rho\alpha}$ with ρ real, the integral in (2.13) gives $H[u](\alpha) = -i \operatorname{sgn}(\rho) e^{i\rho\alpha}$. For extensions to the *upper* half-plane, the sum in (2.9) is over $\langle \mathbf{j}, \mathbf{k} \rangle > 0$, the last formula in (2.10) becomes $\hat{v}_j = -i \operatorname{sgn}(\langle \mathbf{j}, \mathbf{k} \rangle) \hat{u}_j$, and the signs in front of $H[u]$ and $H[v]$ in (2.11) are reversed.

Remark 2.2. As with P and P_0 , there is an analogous operator on $L^2(\mathbb{T}^d)$ such that $H[u](\alpha) = H[\tilde{u}](k\alpha)$. The formula is

$$(2.14) \quad H[\tilde{u}](\alpha) = \sum_{j \in \mathbb{Z}^d} (-i) \operatorname{sgn}(\langle j, k \rangle) \hat{u}_j e^{i\langle j, \alpha \rangle}.$$

If necessary for clarity, one can also write $H_k[\tilde{u}]$ to emphasize the dependence of H on k . H commutes with the shift operator $S_\theta[\tilde{u}](\alpha) = \tilde{u}(\alpha + \theta)$, so if $\tilde{v} = \hat{v}_0 - H[\tilde{u}]$ and $\hat{u}_0 = P_0[\tilde{u}]$, then $v(\alpha; \theta) = \tilde{v}(k\alpha + \theta)$ is related to $u(\alpha; \theta) = \hat{u}(k\alpha + \theta)$ by (2.11). Also, if $f(z)$ in (2.9) is the bounded analytic extension of $u + iv$ (with $\theta = \mathbf{0}$) to the lower half-plane, we have

$$(2.15) \quad f(w) = \tilde{f}(k\alpha, \beta), \quad (w = \alpha + i\beta, \beta \leq 0),$$

where $\tilde{f}(\alpha, \beta) = \hat{u}_0 + i\hat{v}_0 + \sum_{\langle j, k \rangle < 0} 2[\hat{u}_j e^{-\langle j, k \rangle \beta}] e^{i\langle j, \alpha \rangle}$ is periodic in α for fixed $\beta \leq 0$. The bounded analytic extension of $[u(\alpha; \theta) + iv(\alpha; \theta)]$ to the lower half-plane is then given by $f(\alpha + i\beta; \theta) = \tilde{f}(k\alpha + \theta, \beta)$.

2.3. The Conformal Mapping. We consider a time dependent conformal mapping that maps the conformal domain

$$(2.16) \quad \mathbb{C}^- = \{\alpha + i\beta : \alpha \in \mathbb{R}, \beta < 0\}$$

to the fluid domain

$$(2.17) \quad \Omega_f(t) = \{x + iy : x \in \mathbb{R}, y < \eta(x, t)\}.$$

This conformal mapping, denoted by $z(w, t)$, extends continuously to $\overline{\mathbb{C}^-}$ and maps the real line $\beta = 0$ to the free surface

$$(2.18) \quad \Gamma(t) = \{x + iy : y = \eta(x, t)\}.$$

We express $z(w, t)$ as

$$(2.19) \quad z(w, t) = x(w, t) + iy(w, t), \quad (w = \alpha + i\beta).$$

We also introduce the notation $\zeta = z|_{\beta=0}$, $\xi = x|_{\beta=0}$ and $\eta = y|_{\beta=0}$ so that the free surface is parametrized by

$$(2.20) \quad \zeta(\alpha, t) = \xi(\alpha, t) + i\eta(\alpha, t), \quad (\alpha \in \mathbb{R}).$$

This allows us to denote a generic field point in the physical fluid by $z = x + iy$ while simultaneously discussing points $\zeta = \xi + i\eta$ on the free surface. To avoid ambiguity, we will henceforth denote the free surface elevation function from the previous section by $\eta^{\text{phys}}(x, t)$. Thus,

$$(2.21) \quad \eta(\alpha, t) = \eta^{\text{phys}}(\xi(\alpha, t), t), \quad \eta_\alpha = \eta_x^{\text{phys}} \xi_\alpha, \quad \eta_t = \eta_x^{\text{phys}} \xi_t + \eta_t^{\text{phys}}.$$

The parametrization (2.20) is more general than (2.21) in that it allows for overturning waves. In deriving the equations of motion for $\zeta(\alpha, t)$ and $\varphi(\alpha, t)$ in Section 2.5 below, we will indicate the modifications necessary to handle the case of overturning waves. In particular, as discussed in Appendix A, $\Gamma(t)$ is defined in this case as the image of $\zeta(\cdot, t)$, which is assumed to be injective on \mathbb{R} , and $\Omega_f(t)$ can be obtained from $\Gamma(t)$ using a linear fractional transformation and the Jordan curve theorem.

The conformal map is required to remain a bounded distance from the identity map in the lower half-plane. Specifically, we require that

$$(2.22) \quad |z(w, t) - w| \leq M(t) \quad (w = \alpha + i\beta, \beta \leq 0),$$

where $M(t)$ is a uniform bound that could vary in time. The Cauchy integral formula implies that $|z_w - 1| \leq M(t)/|\beta|$, so at any fixed time,

$$(2.23) \quad z_w \rightarrow 1 \quad \text{as} \quad \beta \rightarrow -\infty.$$

Our goal is to investigate the case when the free surface is quasi-periodic in α . This differs from conformal mappings discussed in [16, 18, 30, 44], where it is assumed to be periodic.

In the present work, η is assumed to have two spatial quasi-periods, i.e. at any time it has the form (2.6) with $d = 2$ and $\mathbf{k} = [k_1, k_2]^T$. Since k_1 and k_2 are irrationally related, we assume without loss of generality that $k_1 = 1$ and $k_2 = k$, where k is irrational,

$$(2.24) \quad \eta(\alpha, t) = \tilde{\eta}(\alpha, k\alpha, t), \quad \tilde{\eta}(\alpha_1, \alpha_2, t) = \sum_{j_1, j_2 \in \mathbb{Z}} \hat{\eta}_{j_1, j_2}(t) e^{i(j_1 \alpha_1 + j_2 \alpha_2)}.$$

Here $\hat{\eta}_{-j_1, -j_2}(t) = \overline{\hat{\eta}_{j_1, j_2}(t)}$ since $\tilde{\eta}(\alpha_1, \alpha_2, t)$ is real-valued. Since $w \mapsto [z(w, t) - w]$ is bounded and analytic on \mathbb{C}^- and its imaginary part agrees with η on the real axis, there is a real number x_0 (possibly depending on time) such that

$$(2.25) \quad \xi(\alpha, t) = \alpha + x_0(t) + H[\eta](\alpha, t).$$

Using (2.23) and $\text{Im}[z_w|_{\beta=0}] = \eta_\alpha$ or differentiating (2.25) gives

$$(2.26) \quad \xi_\alpha(\alpha, t) = 1 + H[\eta_\alpha](\alpha, t).$$

We use a tilde to denote the periodic functions on the torus that correspond to the quasi-periodic parts of ξ , ζ and z ,

$$(2.27) \quad \begin{aligned} \xi(\alpha, t) &= \alpha + \tilde{\xi}(\alpha, k\alpha, t), & \zeta(\alpha, t) &= \alpha + \tilde{\zeta}(\alpha, k\alpha, t), \\ z(\alpha + i\beta, t) &= (\alpha + i\beta) + \tilde{z}(\alpha, k\alpha, \beta, t), & (\beta \leq 0). \end{aligned}$$

Specifically, $\tilde{\xi} = x_0(t) + H[\tilde{\eta}]$ in the sense of Remark 2.2, $\tilde{\zeta} = \tilde{\xi} + i\tilde{\eta}$, and

$$(2.28) \quad \tilde{z}(\alpha_1, \alpha_2, \beta, t) = x_0(t) + i\hat{\eta}_{0,0}(t) + \sum_{j_1 + j_2 k < 0} \left(2i\hat{\eta}_{j_1, j_2}(t) e^{-(j_1 + j_2 k)\beta} \right) e^{i(j_1 \alpha_1 + j_2 \alpha_2)}.$$

While the mean surface height remains constant in physical space, $\hat{\eta}_{0,0}(t)$ generally varies in time. Since the modes $\hat{\eta}_{j_1, j_2}$ are assumed to decay exponentially, there is a uniform bound $M(t)$ such that $|\tilde{z}(\alpha_1, \alpha_2, \beta, t)| \leq M(t)$ for $(\alpha_1, \alpha_2) \in \mathbb{T}^2$ and $\beta \leq 0$. In Appendix A we show that as long as the free surface $\tilde{\zeta}(\alpha, t)$ does not self-intersect at a given time t , the mapping $w \mapsto z(w, t)$ is an analytic isomorphism of the lower half-plane onto the fluid region.

2.4. The Complex Velocity Potential. Let $\Phi^{\text{phys}}(x, y, t)$ denote the velocity potential in physical space from Section 2.1 above and let $W^{\text{phys}}(x + iy, t) = \Phi^{\text{phys}}(x, y, t) + i\Psi^{\text{phys}}(x, y, t)$ be the complex velocity potential, where Ψ^{phys} is the stream function. Using the conformal mapping (2.19), we pull back these functions to the lower half-plane and define

$$W(w, t) = \Phi(\alpha, \beta, t) + i\Psi(\alpha, \beta, t) = W^{\text{phys}}(z(w, t), t), \quad (w = \alpha + i\beta).$$

We also define $\varphi = \Phi|_{\beta=0}$ and $\psi = \Psi|_{\beta=0}$ and use (2.5) and (2.21) to obtain

$$(2.29) \quad \varphi(\alpha, t) = \varphi^{\text{phys}}(\xi(\alpha, t), t), \quad \psi(\alpha, t) = \psi^{\text{phys}}(\xi(\alpha, t), t),$$

where $\psi^{\text{phys}}(x, t) = \Psi^{\text{phys}}(x, \eta^{\text{phys}}(x, t), t)$. We assume φ is quasi-periodic with the same quasi-periods as η ,

$$\varphi(\alpha, t) = \tilde{\varphi}(\alpha, k\alpha, t), \quad \tilde{\varphi}(\alpha_1, \alpha_2, t) = \sum_{j_1, j_2 \in \mathbb{Z}} \hat{\varphi}_{j_1, j_2}(t) e^{i(j_1 \alpha_1 + j_2 \alpha_2)}.$$

The fluid velocity $\nabla\Phi^{\text{phys}}(x, y, t)$ is assumed to decay to zero as $y \rightarrow -\infty$ (since we work in the lab frame). From (2.23) and (2.31) below, $dW/dw \rightarrow 0$ as $\beta \rightarrow -\infty$. Thus, $\psi_\alpha = -H[\varphi_\alpha]$. Writing this as $\partial_\alpha[\psi + H\varphi] = 0$, we conclude that

$$(2.30) \quad \psi(\alpha, t) = -H[\varphi](\alpha, t).$$

Here we have set the integration constant to zero and assumed $P_0[\varphi] = \hat{\varphi}_{0,0}(t) = 0$ and $P_0[\psi] = \hat{\psi}_{0,0}(t) = 0$, which is allowed since Φ and Ψ can be modified by additive constants (or functions of time only) without affecting the fluid motion.

2.5. Governing Equations in Conformal Space. Loosely following [11, 16, 44], we now present a derivation of the equations of motion for surface water waves in a conformal mapping formulation and show how to handle quasi-periodic solutions.

From the chain rule,

$$(2.31) \quad \frac{dW}{dw} = \frac{dW^{\text{phys}}}{dz} \cdot \frac{dz}{dw} \quad \Rightarrow \quad \Phi_x^{\text{phys}} + i\Psi_x^{\text{phys}} = \frac{\Phi_\alpha + i\Psi_\alpha}{x_\alpha + iy_\alpha}.$$

Evaluating (2.31) on the free surface gives

$$(2.32) \quad \Phi_x^{\text{phys}} = \frac{\varphi_\alpha \xi_\alpha + \psi_\alpha \eta_\alpha}{J}, \quad \Phi_y^{\text{phys}} = -\Psi_x^{\text{phys}} = \frac{\varphi_\alpha \eta_\alpha - \psi_\alpha \xi_\alpha}{J}, \quad J = \xi_\alpha^2 + \eta_\alpha^2.$$

Using (2.21) and (2.32) in (2.3) and multiplying by ξ_α , we obtain

$$(2.33) \quad \eta_t \xi_\alpha - \xi_t \eta_\alpha = -\psi_\alpha.$$

This states that the normal velocity of the free surface is equal to the normal velocity of the fluid, $\hat{\mathbf{n}} \cdot (\xi_t, \eta_t) = \hat{\mathbf{n}} \cdot \nabla\Phi^{\text{phys}}$, where $\hat{\mathbf{n}} = (-\eta_\alpha, \xi_\alpha)/\sqrt{J}$. This can also be obtained by tracking a fluid particle $x_p(t) + iy_p(t) = \zeta(\alpha_p(t), t)$ on the free surface. We have $\dot{x}_p = \xi_\alpha \dot{\alpha}_p + \xi_t = \Phi_x^{\text{phys}}$ and $\dot{y}_p = \eta_\alpha \dot{\alpha}_p + \eta_t = \Phi_y^{\text{phys}}$, which leads to (2.33) after eliminating $\dot{\alpha}_p$. This argument does not assume the free surface is a graph, i.e. (2.33) is also valid for overturning waves.

Next we define a new function,

$$(2.34) \quad q := \frac{\zeta_t}{\zeta_\alpha} = \frac{(\xi_t \xi_\alpha + \eta_t \eta_\alpha) + i(\eta_t \xi_\alpha - \xi_t \eta_\alpha)}{J} = \frac{(\xi_t \xi_\alpha + \eta_t \eta_\alpha) - i\psi_\alpha}{J}.$$

Since q is quasi-periodic in α and extends analytically to the lower half-plane via z_t/z_α , the real and imaginary part of q can be related by the Hilbert transform. Here we have assumed that z_t/z_α is bounded, which will be justified below. Thus,

$$(2.35) \quad \frac{\xi_t \xi_\alpha + \eta_t \eta_\alpha}{J} = -H \left[\frac{\psi_\alpha}{J} \right] + C_1,$$

where C_1 is an arbitrary integration constant that may depend on time but not space. Let $\hat{\mathbf{s}} = (\xi_\alpha, \eta_\alpha)/\sqrt{J}$ denote the unit tangent vector to the curve. Equation (2.35) prescribes the tangential velocity $\hat{\mathbf{s}} \cdot (\xi_t, \eta_t)$ of points on the curve in terms of the normal velocity in order to maintain a conformal parametrization. Note that the tangent velocity of the curve differs from that of the underlying fluid particles. This is similar in spirit to a method of Hou, Lowengrub and Shelley [22, 23], who proposed a tangential velocity that maintains a uniform parametrization of the curve (rather than a conformal one); see also [3, 41].

Combining (2.33) and (2.35), we obtain the kinematic boundary conditions in conformal space,

$$(2.36) \quad \begin{pmatrix} \xi_t \\ \eta_t \end{pmatrix} = \begin{pmatrix} \xi_\alpha & -\eta_\alpha \\ \eta_\alpha & \xi_\alpha \end{pmatrix} \begin{pmatrix} -H \left[\frac{\psi_\alpha}{J} \right] + C_1 \\ -\frac{\psi_\alpha}{J} \end{pmatrix}.$$

The right-hand side can be interpreted as complex multiplication of z_α with z_t/z_α . Since both functions are analytic in the lower half-plane, their product is, too. Thus, ξ_t is related to η_t via the Hilbert transform (up to a constant). The constant is determined by comparing (2.25) with (2.36), which gives

$$(2.37) \quad \frac{dx_0}{dt} = P_0 \left[\xi_\alpha \left(-H \left[\frac{\psi_\alpha}{J} \right] + C_1 \right) + \frac{\eta_\alpha \psi_\alpha}{J} \right].$$

The three most natural choices of C_1 are

$$(2.38) \quad \begin{aligned} (a) \quad C_1 = 0 &: && \text{evolve } x_0(t) \text{ via (2.37),} \\ (b) \quad C_1 = P_0 [\xi_\alpha H[\psi_\alpha/J] - \eta_\alpha \psi_\alpha/J] &: && x_0(t) = 0, \\ (c) \quad C_1 = [H[\psi_\alpha/J] - \eta_\alpha \psi_\alpha/(\xi_\alpha J)]_{\alpha=0} &: && \xi(0, t) = 0. \end{aligned}$$

In options (b) and (c), the evolution equation ensures that $dx_0/dt = 0$ and $\xi_t(0, t) = 0$, respectively, so we have assumed the initial conditions satisfy $x_0(0) = 0$ or $\xi(0, 0) = 0$. Option (c) amounts to setting $x_0(t) = -H[\eta](0, t)$ in (2.25). This arguably leads to the most natural parametrization, but would have a problem if the vertical part of an overturning wave crosses $\alpha = 0$. Indeed, such a crossing would lead to $\xi_\alpha(0, t) = 0$ at some time t in the denominator of (2.38c). For overturning waves, we recommend option (b).

Next we evaluate the Bernoulli equation $\Phi_t^{\text{phys}} + \frac{1}{2} |\nabla \Phi^{\text{phys}}|^2 + \frac{p}{\rho} + gy = C_2$ at the free surface to obtain an evolution equation for $\varphi(\alpha, t)$. Here C_2 is an arbitrary integration constant that may depend on time but not space. The pressure at the free surface is determined by the Laplace-Young condition, $p = p_0 - \rho\tau\kappa$, where κ is the curvature, $\rho\tau$ is the surface tension, and p_0 is a constant that can be absorbed into C_2 and set to zero. From (2.31) or (2.32), we know $|\nabla \Phi^{\text{phys}}|^2 = (\varphi_\alpha^2 + \psi_\alpha^2)/J$ on the free surface. Finally, differentiating $\varphi(\alpha, t) = \Phi^{\text{phys}}(\xi(\alpha, t), \eta(\alpha, t), t)$ and using (2.32) and (2.36), we obtain

$$(2.39) \quad \varphi_t = \underbrace{\left(\Phi_x^{\text{phys}}, \Phi_y^{\text{phys}} \right)}_{(\varphi_\alpha, -\psi_\alpha)} \begin{pmatrix} \xi_\alpha & -\eta_\alpha \\ \eta_\alpha & \xi_\alpha \end{pmatrix} \begin{pmatrix} -H[\psi_\alpha/J] + C_1 \\ -\psi_\alpha/J \end{pmatrix} - \frac{\varphi_\alpha^2 + \psi_\alpha^2}{2J} - g\eta + \tau\kappa + C_2.$$

We choose C_2 so that $P_0[\varphi_t] = 0$. In conclusion, we obtain the following governing equations for spatially quasi-periodic gravity-capillary waves in conformal space

$$(2.40) \quad \begin{aligned} \xi_\alpha &= 1 + H[\eta_\alpha], & \psi &= -H[\varphi], & J &= \xi_\alpha^2 + \eta_\alpha^2, & \chi &= \frac{\psi_\alpha}{J}, \\ \text{choose } C_1, \text{ e.g. as in (2.38),} & & \text{compute } \frac{dx_0}{dt} & \text{ in (2.37) if necessary,} & & & & \\ \eta_t &= -\eta_\alpha H[\chi] - \xi_\alpha \chi + C_1 \eta_\alpha, & \kappa &= \frac{\xi_\alpha \eta_{\alpha\alpha} - \eta_\alpha \xi_{\alpha\alpha}}{J^{3/2}}, & & & & \\ \varphi_t &= P \left[\frac{\psi_\alpha^2 - \varphi_\alpha^2}{2J} - \varphi_\alpha H[\chi] + C_1 \varphi_\alpha - g\eta + \tau\kappa \right]. & & & & & & \end{aligned}$$

Note that these equations govern the evolution of x_0 , η and φ , which determine the state of the system. The functions ξ , ψ , J , χ and κ are determined at any moment by x_0 , η and φ through the auxiliary equations in (2.40). We emphasize that C_1 can be chosen arbitrarily as long as dx_0/dt satisfies (2.37). The special cases (2.38b) and (2.38c) lead to nice formulas for $x_0(t)$ without having to evolve (2.37) numerically.

In deriving (2.40) from (2.33) and (2.39), we had to assume z_t/z_α remains bounded in the lower half-plane. Conditions that ensure the boundedness of $1/z_\alpha$ are given in Appendix A. We note that z_t/z_α is automatically bounded in the converse direction, where (2.33) and (2.39) are derived from (2.40). In more detail, when solving (2.40), z_t/z_α is constructed first, before z_t , as the bounded extension of the quasi-periodic function with imaginary part $(-\psi_\alpha/J)$ to the lower half-plane. Equation (2.36) then defines z_t as the product of this function by z_α , which is also bounded since $\xi_\alpha = 1 + H[\eta_\alpha]$. Thus, the first component of each side of (2.36) is related to the corresponding second component by the Hilbert transform, up to a constant. Since the second components are equal (i.e. the η_t equation holds), the ξ_t equation also holds — the constants are accounted for by (2.37). Left-multiplying (2.36) by the row vector $[-\eta_\alpha, \xi_\alpha]$ gives the kinematic condition (2.33), as required.

Equations (2.40) break down if J becomes zero somewhere on the curve. Such a singularity would arise, for example, if the wave profile were to form a corner in finite time. To our knowledge, it remains an open question whether the free-surface Euler equations can form such a corner.

Often we wish to verify that a given curve $\zeta(\alpha, t) = \xi(\alpha, t) + i\eta(\alpha, t)$ and velocity potential $\varphi(\alpha, t)$ satisfy the conformal version of the water wave equations. We say that (ζ, φ) satisfy (2.40) if ξ and η remain conformally related via (2.25), which determines $x_0(t)$, and if x_0 , η and φ satisfy (2.40) with $C_1(t)$ obtained from (2.37) using $P_0[\xi_\alpha] = 1$. As noted above, these equations imply the kinematic condition (2.33) and Bernoulli equation (2.39). If necessary, one should replace the given $\varphi(\alpha, t)$ by $P[\varphi(\cdot, t)]$ before checking that (2.40) is satisfied.

Remark 2.3. Equations (2.40) can be interpreted as an evolution equation for the functions $\tilde{\zeta}(\alpha_1, \alpha_2, t)$ and $\tilde{\varphi}(\alpha_1, \alpha_2, t)$ on the torus \mathbb{T}^2 . The α -derivatives are replaced by the directional derivatives $[\partial_{\alpha_1} + k\partial_{\alpha_2}]$ and, as noted in Remark 2.2 above, the Hilbert transform becomes a two-dimensional Fourier multiplier operator with symbol $(-i) \operatorname{sgn}(j_1 + j_2k)$. The pseudo-spectral method we propose in Section 3 below is based on this representation. Equation (2.38c) becomes

$$(2.41) \quad C_1 = \left[H \left(\frac{\tilde{\psi}_\alpha}{\tilde{J}} \right) - \frac{\tilde{\eta}_\alpha \tilde{\psi}_\alpha}{(1 + \tilde{\xi}_\alpha) \tilde{J}} \right]_{(\alpha_1, \alpha_2) = (0, 0)}, \quad \tilde{\xi}(0, 0, t) = 0,$$

where $\tilde{J} = (1 + \tilde{\xi}_\alpha)^2 + \tilde{\eta}_\alpha^2$. Note that ξ_α in (2.40) is replaced by

$$(2.42) \quad \tilde{\xi}_\alpha = 1 + \tilde{\xi}_\alpha,$$

which is the one place this notation becomes awkward. Using (2.25) and (2.27), $\tilde{\zeta}$ is completely determined by $x_0(t)$ and $\tilde{\eta}$, so only these have to be evolved — the formula for $\tilde{\xi}_t$ in (2.36) is redundant as long as (2.37) is satisfied. If both components of $\tilde{\zeta}(\alpha_1, \alpha_2, t)$ are given, we say that $(\tilde{\zeta}, \tilde{\varphi})$ satisfy the torus version of (2.40) if there is a continuously

differentiable function $x_0(t)$ such that $\tilde{\xi} = x_0(t) + H[\tilde{\eta}]$ and if x_0 , $\tilde{\eta}$ and $\tilde{\varphi}$ satisfy the torus version of (2.40) with $C_1 = dx_0/dt + P_0[(1 + \tilde{\xi}_\alpha)H[\tilde{\psi}_\alpha/\tilde{J}] - \tilde{\eta}_\alpha\tilde{\psi}_\alpha/\tilde{J}]$.

We show in Appendix B that solving the torus version of (2.40) yields a three-parameter family of one-dimensional solutions of the form

$$(2.43) \quad \begin{aligned} \zeta(\alpha, t; \theta_1, \theta_2, \delta) &= \alpha + \delta + \tilde{\zeta}(\theta_1 + \alpha, \theta_2 + k\alpha, t), \\ \varphi(\alpha, t; \theta_1, \theta_2) &= \tilde{\varphi}(\theta_1 + \alpha, \theta_2 + k\alpha, t), \end{aligned} \quad \left(\begin{array}{l} \alpha \in \mathbb{R}, t \geq 0 \\ \theta_1, \theta_2, \delta \in \mathbb{R} \end{array} \right).$$

We also show that if all the waves in this family are single-valued and have no vertical tangent lines, there is a corresponding family of solutions of the Euler equations in the original graph-based formulation of (2.1)–(2.4) that are quasi-periodic in physical space. A precise statement is given in Theorem B.2.

3. NUMERICAL METHOD

In this section, we describe a pseudo-spectral time-stepping strategy for evolving water waves with spatially quasi-periodic initial conditions. The evolution equations (2.40) for η and φ are nonlinear and involve computing derivatives, antiderivatives and Hilbert transforms of quasi-periodic functions. Let f denote one of these functions (e.g. η , φ or χ) and let \tilde{f} denote the corresponding periodic function on the torus,

$$(3.1) \quad f(\alpha) = \tilde{f}(\alpha, k\alpha), \quad \tilde{f}(\alpha_1, \alpha_2) = \sum_{j_1, j_2 \in \mathbb{Z}} \hat{f}_{j_1, j_2} e^{i(j_1\alpha_1 + j_2k\alpha_2)}, \quad (\alpha_1, \alpha_2) \in \mathbb{T}^2.$$

The functions f_α and $H[f]$ then correspond to

$$(3.2) \quad \begin{aligned} \tilde{f}_\alpha(\alpha_1, \alpha_2) &= \sum_{j_1, j_2 \in \mathbb{Z}} i(j_1 + j_2k) \hat{f}_{j_1, j_2} e^{i(j_1\alpha_1 + j_2k\alpha_2)}, \\ \widetilde{H[f]}(\alpha_1, \alpha_2) &= \sum_{j_1, j_2 \in \mathbb{Z}} (-i) \operatorname{sgn}(j_1 + j_2k) \hat{f}_{j_1, j_2} e^{i(j_1\alpha_1 + j_2k\alpha_2)}. \end{aligned}$$

We propose a pseudo-spectral method in which each such f that arises in the formulas (2.40) is represented by the values of \tilde{f} at $M_1 \times M_2$ equidistant gridpoints on the torus \mathbb{T}^2 ,

$$(3.3) \quad \tilde{f}_{m_1, m_2} = \tilde{f}(2\pi m_1/M_1, 2\pi m_2/M_2), \quad (0 \leq m_1 < M_1, 0 \leq m_2 < M_2).$$

We visualize a 90° rotation between the matrix \tilde{F} holding the entries \tilde{f}_{m_1, m_2} and the collocation points in the torus. The columns of the matrix correspond to horizontal slices of gridpoints while the rows of the matrix correspond to vertical slices indexed from bottom to top. The nonlinear operations in (2.40) consist of products, powers and division; they are carried out pointwise on the grid. Derivatives and the Hilbert transform are computed in Fourier space via (3.2). To plot the solution, we also need to compute an antiderivative to get ξ from $f = \xi_\alpha$. This involves dividing \hat{f}_{j_1, j_2} by $i(j_1 + j_2k)$ when $(j_1, j_2) \neq (0, 0)$ and adjusting the $(0, 0)$ mode to obtain $\xi(0, t) = 0$.

Since the functions f that arise in the computation are real-valued, we use the real-to-complex ('r2c') version of the two-dimensional discrete Fourier transform. The 'r2c' transform of a one-dimensional array of length M (assumed even) is given by

$$(3.4) \quad \{g_m\}_{m=0}^{M-1} \mapsto \{\hat{g}_j\}_{j=0}^{M/2}, \quad \hat{g}_j = \frac{1}{M} \sum_{m=0}^{M-1} g_m e^{-2\pi i j m / M}.$$

In practice, the \hat{g}_j are computed simultaneously in $O(M \log M)$ time rather than by this formula. The fully complex ('c2c') transform of this (real) data would give additional values \hat{g}_j with $M/2 + 1 \leq j \leq M - 1$. These extra entries are actually aliased values of negative-index modes; they are redundant due to $\hat{g}_j = \hat{g}_{j-M} = \overline{\hat{g}_{M-j}}$. Since the imaginary components of \hat{g}_0 and $\hat{g}_{M/2}$ are zero, the number of real degrees of freedom on both sides of (3.4) is M . The Nyquist mode $\hat{g}_{M/2}$ requires special attention. Setting $\hat{g}_{M/2} = 1$ and the other modes to zero yields $g_m = \cos(\pi m) = (-1)^m$. The derivative and Hilbert transform of this mode are taken to be zero since they would involve evaluating $\sin(M\alpha/2)$ at the gridpoints $\alpha_m = 2\pi m/M$.

The two-dimensional 'r2c' transform can be computed by applying one-dimensional 'r2c' transforms in the x -direction (i.e. to the columns of \tilde{F}) followed by one-dimensional 'c2c' transforms in the y -direction (i.e. to the rows of \tilde{F}):

$$(3.5) \quad \hat{f}_{j_1, j_2} = \frac{1}{M_2} \sum_{m_2=0}^{M_2-1} \left(\frac{1}{M_1} \sum_{m_1=0}^{M_1-1} \tilde{f}_{m_1, m_2} e^{-2\pi i j_1 m_1 / M_1} \right) e^{-2\pi i j_2 m_2 / M_2}, \quad \left(\begin{array}{l} 0 \leq j_1 \leq M_1/2 \\ -M_2/2 < j_2 \leq M_2/2 \end{array} \right).$$

The 'r2c' routine in the FFTW library actually returns the index range $0 \leq j_2 < M_2$, but we use $\hat{f}_{j_1, j_2 - M_2} = \hat{f}_{j_1, j_2}$ to de-alias the Fourier modes and map the indices $j_2 > M_2/2$ to their correct negative values. The missing entries with $-M_1/2 < j_1 < 0$ are determined implicitly by

$$(3.6) \quad \hat{f}_{-j_1, -j_2} = \overline{\hat{f}_{j_1, j_2}}.$$

This imposes additional constraints on the computed Fourier modes, namely

$$(3.7) \quad \begin{aligned} \text{Im}\{\hat{f}_{0,0}\} &= 0, & \text{Im}\{\hat{f}_{M_1/2,0}\} &= 0, & \text{Im}\{\hat{f}_{0,M_2/2}\} &= 0, & \text{Im}\{\hat{f}_{M_1/2,M_2/2}\} &= 0, \\ \hat{f}_{0,-j_2} &= \overline{\hat{f}_{0,j_2}}, & \hat{f}_{M_1/2,-j_2} &= \overline{\hat{f}_{M_1/2,j_2}}, & & & & (1 \leq j_2 \leq M_2/2 - 1), \end{aligned}$$

where we also used $\hat{f}_{-M_1/2, j_2} = \hat{f}_{M_1/2, j_2}$. This reduces the number of real degrees of freedom in the complex $(M_1/2 + 1) \times M_2$ array of Fourier modes to $M_1 M_2$. When computing f_α and $H[f]$ via (3.2), the Nyquist modes with $j_1 = M_1/2$ or $j_2 = M_2/2$ are set to zero. Otherwise the formulas (3.2) respect the constraints (3.7) and the 'c2r' transform reconstructs real-valued functions \widetilde{f}_α and $\widetilde{H}[f]$ from their Fourier modes.

The evolution equations (2.40) are not stiff when the surface tension parameter is small or vanishes, but become moderately stiff for larger values of τ . We find that the 5th and 8th order explicit Runge-Kutta methods of Dormand and Prince [20] work well for smaller values of τ , and exponential time-differencing (ETD) methods [7, 10, 12, 24, 37] work well generally. In the ETD framework, we follow the basic idea of the small-scale decomposition for removing stiffness from interfacial flows [22, 23] and write the equations in the form

$$(3.8) \quad \begin{pmatrix} \eta_t \\ \varphi_t \end{pmatrix} = L \begin{pmatrix} \eta \\ \varphi \end{pmatrix} + \mathcal{N}, \quad L = \begin{pmatrix} 0 & H\partial_\alpha \\ -(gP - \tau\partial_{\alpha\alpha}) & 0 \end{pmatrix},$$

where P is the projection in (2.8), H is the Hilbert transform in (2.12), and

$$(3.9) \quad \mathcal{N} = \begin{pmatrix} -\eta_\alpha H[\chi] - (\xi_\alpha \chi - \psi_\alpha) + C_1 \eta_\alpha \\ P \left[\frac{\psi_\alpha^2 - \varphi_\alpha^2}{2J} - \varphi_\alpha H[\chi] + C_1 \varphi_\alpha + \tau(\kappa - \eta_{\alpha\alpha}) \right] \end{pmatrix}.$$

Note that \mathcal{N} is obtained by subtracting the terms included in L from (2.40), e.g. $H\partial_\alpha\varphi = -\psi_\alpha$. The eigenvalues of L are $\pm i\sqrt{|j_1 + j_2k|[g + \tau(j_1 + j_2k)^2]}$, so the leading source of stiffness is dispersive. This $3/2$ power growth rate of the eigenvalues of the leading dispersive term with respect to wave number is typical of interfacial fluid flows with surface tension [22, 23]. For stiffer problems such as the Benjamin-Ono and KdV equations, the growth rate is faster (quadratic and cubic, respectively) and it becomes essential to use a semi-implicit or exponential time-differencing scheme to avoid severe time-stepping restrictions. Here it is less critical, but still useful. Further details on how to implement (3.8) and (3.9) in the ETD framework will be given elsewhere [10].

In both the explicit Runge-Kutta and ETD methods, as explained above, the functions evolved in time are $\tilde{\eta}(\alpha_1, \alpha_2, t)$ and $\tilde{\varphi}(\alpha_1, \alpha_2, t)$, sampled on the uniform $M_1 \times M_2$ grid covering \mathbb{T}^2 . At the end of each time step, our code can (optionally) apply a 36th order filter [21, 22] with Fourier multiplier $\exp(-36[(2j_1/M_1)^{36} + (2j_2/M_2)^{36}])$. In all the computations reported below, we used the same number of gridpoints in the x and y -directions, $M_1 = M_2 = M$. The filter has almost no effect on these results since the Fourier modes decay to machine precision before the filter deviates appreciably from 1.

4. NUMERICAL RESULTS

In this section, we compute spatially quasi-periodic solutions of the initial value problem (2.40) with $k = 1/\sqrt{2}$ and g normalized to 1. First we validate the traveling wave computations of [41] and compare the accuracy and efficiency of the ERK and ETD schemes in a convergence study. We then consider more complex dynamics in which some of the waves overturn.

4.1. Traveling waves. Figure 1 shows the time evolution from $t = 0$ to $t = 3$ of a traveling wave computed at $t = 0$ by the algorithm of [41] with amplitude parameters $\hat{\eta}_{1,0} = 0.01$ and $\hat{\eta}_{0,1} = 0.01$. It also shows the error at the final time for various choices of time-stepping scheme and number of time steps. Panel (a) shows snapshots of the solution in the lab frame at equal time intervals of size $\Delta t = 0.1$. The initial condition is plotted with a thick blue line, and the wave travels right at constant speed $c = 1.552197$ in physical space. The solution is plotted over the representative interval $0 \leq x \leq 12\pi$, though it extends in both directions to $\pm\infty$ without exactly repeating.

Panel (b) shows the error in time-stepping this traveling wave solution from $t = 0$ to $t = 3$ using the 5th and 8th order explicit Runge-Kutta methods of Dormand and Prince [20], the 4th order ETD scheme of Cox and Matthews [12, 24], and the 5th order ETD scheme of Whalen, Brio and Moloney [37]. These errors compare the numerical solution from time-stepping the initial condition to the exact formula of how a quasi-periodic traveling wave should evolve under (2.40) and (2.41), which is worked out in [41]. If the initial wave profile has the torus representation $\tilde{\eta}_0(\alpha_1, \alpha_2)$, we define $\tilde{\xi}_0 = H[\tilde{\eta}_0]$ and $\tilde{\varphi}_0 = c\tilde{\xi}_0$. We assume $\tilde{\eta}_0$ is an even function of $\alpha = (\alpha_1, \alpha_2)$, so $\tilde{\xi}_0$ and $\tilde{\varphi}_0$ are odd. The exact traveling solution is then

$$(4.1) \quad \begin{aligned} \tilde{\eta}_{\text{exact}}(\alpha_1, \alpha_2, t) &= \tilde{\eta}_0(\alpha_1 - \alpha_0(t), \alpha_2 - k\alpha_0(t)), \\ \tilde{\varphi}_{\text{exact}}(\alpha_1, \alpha_2, t) &= \tilde{\varphi}_0(\alpha_1 - \alpha_0(t), \alpha_2 - k\alpha_0(t)), \end{aligned}$$

where $\alpha_0(t) = ct - \mathcal{A}(-ct, -kct)$ and $\mathcal{A}(x_1, x_2)$ is a periodic function on \mathbb{T}^2 defined implicitly by (B.7) below. The waves in (4.1) do not change shape as they move through the

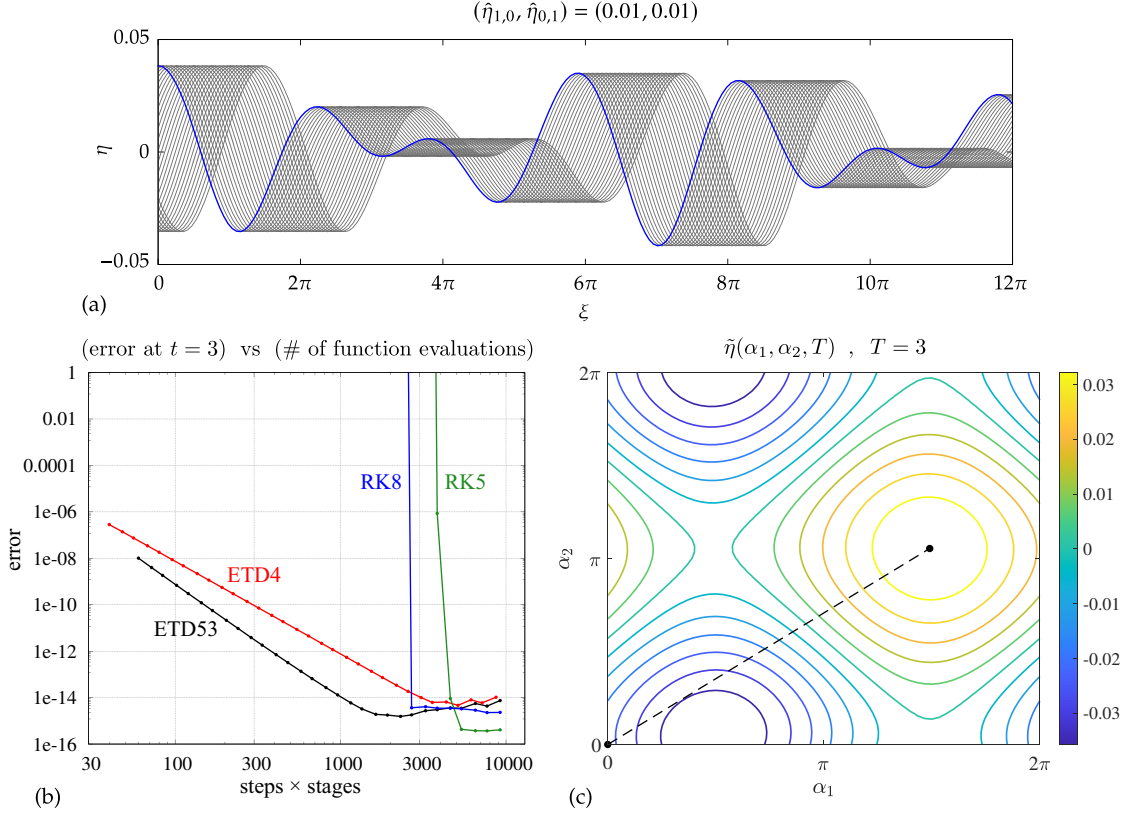


FIGURE 1. Time evolution of a quasi-periodic traveling water wave computed in [41] and a convergence plot comparing the accuracy and efficiency of the proposed time-stepping schemes.

torus in the direction $(1, k)$, but the traveling speed $\alpha'_0(t)$ in conformal space varies in time in order to maintain $\xi(0, 0, t) = 0$ via (2.41). The error plotted in panel (b) is the discrete norm at the final time computed, $T = 3$:

$$\text{err} = \sqrt{\|\tilde{\eta} - \tilde{\eta}_{\text{exact}}\|^2 + \|\tilde{\varphi} - \tilde{\varphi}_{\text{exact}}\|^2}, \quad \|\tilde{\eta}\|^2 = \frac{1}{M_1 M_2} \sum_{m_1, m_2} \tilde{\eta} \left(\frac{2\pi m_1}{M_1}, \frac{2\pi m_2}{M_2}, T \right)^2.$$

The surface tension in this example ($\tau = 1.410902$) is high enough that once the stepsize is sufficiently small for Runge-Kutta methods to be stable, roundoff error dominates truncation error. So the errors suddenly drop from very large values (10^{20} or more) to machine precision. By contrast, the error in the ETD methods decays steadily as the stepsize is reduced, indicating that the small-scale decomposition introduced in (3.8) is successful in removing stiffness from the equations of motion [22, 23].

A contour plot of $\tilde{\eta}(\alpha_1, \alpha_2, T)$ at $t = T = 3$ is shown in panel (c) of Figure 1. The dashed line shows the trajectory from $t = 0$ to $t = 3$ of the wave crest that begins at $(0, 0)$ and continues along the path $\alpha_1 = \alpha_0(t)$, $\alpha_2 = k\alpha_0(t)$. We use Newton's method to solve the implicit equation (B.7) for $\mathcal{A}(x_1, x_2)$ at each point of the pseudo-spectral grid. We then use FFTW to compute the 2d Fourier representation of $\mathcal{A}(x_1, x_2)$, which can then be used to quickly evaluate the function at any point. We find that the Fourier modes of \mathcal{A} decay

to machine precision on the $M \times M$ grid with $M = 60$, corroborating the assertion in Theorem B.2 below that \mathcal{A} is real analytic.

4.2. Overturning waves. Next we present a spatially quasi-periodic water wave computation in which some of the waves overturn as they evolve while others flatten out. For simplicity, we set the surface tension parameter, τ , to zero. We first seek spatially periodic dynamics in which the initial wave profile has a vertical tangent line that overturns when evolved forward in time and flattens out when evolved backward in time. Through trial and error, we selected the following parametric curves for the initial wave profile and velocity potential of this auxiliary periodic problem:

$$(4.2) \quad \xi_1(\sigma) = \sigma + \frac{3}{5} \sin \sigma - \frac{1}{5} \sin 2\sigma, \quad \eta_1(\sigma) = -(1/2) \cos(\sigma + \pi/2.5), \\ \varphi_1(\sigma) = -(1/2) \cos(\sigma + \pi/4).$$

Note that $\xi_1'(\sigma) = 0$ when $\sigma \in \pi + 2\pi\mathbb{Z}$, and otherwise $\xi_1'(\sigma) > 0$. Thus, vertical tangent lines occur where $\xi_1(\sigma) \in \pi + 2\pi\mathbb{Z}$ and $\eta_1(\sigma) = -0.5 \cos(1.4\pi) = 0.154508$; see Figure 2.

To convert (4.2) to a conformal parametrization, we search for 2π -periodic functions $\eta_2(\alpha)$ and $B_2(\alpha)$ and a number x_2 such that

$$(4.3) \quad \alpha + x_2 + H[\eta_2](\alpha) = \xi_1(\alpha + B_2(\alpha)), \quad \eta_2(\alpha) = \eta_1(\alpha + B_2(\alpha)), \quad B_2(0) = 0.$$

First we solve a simpler variant in which x_2 is absent and $B_2(0)$ is unspecified. Specifically, we solve $\alpha + H[\eta_3](\alpha) = \xi_1(\alpha + B_3(\alpha))$, $\eta_3(\alpha) = \eta_1(\alpha + B_3(\alpha))$ for $\eta_3(\alpha)$ and $B_3(\alpha)$ on a uniform grid with M gridpoints on $[0, 2\pi)$ using Newton's method. The Hilbert transform is computed with spectral accuracy in Fourier space. We then define x_2 as the solution of $x_2 + B_3(x_2) = 0$ that is smallest in magnitude. We solve this equation by a combination of root bracketing and Newton's method; the result is $x_2 = 0.393458$. Finally, we define $B_2(\alpha) = x_2 + B_3(\alpha + x_2)$ and $\eta_2(\alpha) = \eta_3(\alpha + x_2)$, which satisfy (4.3). As shown in Figure 2, the initial conditions $\eta_2(\alpha)$ and $\varphi_2(\alpha) = \varphi_1(\alpha + B_2(\alpha))$ have the desired property that the wave overturns when evolved forward in time via the conformal mapping formulation of the water wave equations and flattens out when evolved backward in time.

We turn this into a quasi-periodic solution by defining initial conditions on the torus of the form

$$(4.4) \quad \tilde{\eta}_0(\alpha_1, \alpha_2) = \eta_2(\alpha_1), \quad \tilde{\varphi}_0(\alpha_1, \alpha_2) = \varphi_2(\alpha_1) \cos(\alpha_2 - q),$$

where q is a free parameter that we choose heuristically to be $q = 0.6k\pi = 1.3329$ in order to make the first wave crest to the right of the origin behave similarly to the periodic 1d solution of Figure 2. (This will be explained below).

The results of the quasi-periodic calculation are summarized in Figures 3 and 4. Panel (a) of Figure 3 shows snapshots of the solution at $t = (\ell/6)T$ for $0 \leq \ell \leq 6$ over the range $0 \leq \xi(\alpha) \leq 16\pi$, where $T = 0.225$. The initial wave profile, $\zeta_0(\alpha) = \xi_0(\alpha) + i\eta_0(\alpha)$ with $\eta_0(\alpha) = \tilde{\eta}_0(\alpha, k\alpha)$, is plotted with a thick blue line. The wave profile is plotted with a thick black line at $t = T$ and with thin grey lines at intermediate times. Panel (b) zooms in on the first wave in panel (a), which overturns as the wave crest moves up and right while the wave trough moves down and left, as indicated by the blue arrows. This is very similar (by design) to the forward evolution of the auxiliary periodic wave of Figure 2, with initial conditions $\eta_2(\alpha)$, $\varphi_2(\alpha)$. Panels (c) and (d) zoom in on two other waves from panel (a) that flatten out (rather than overturn) as t advances from 0 to T . Panel (e) shows another type of behavior in which the wave overturns due to the wave trough moving down

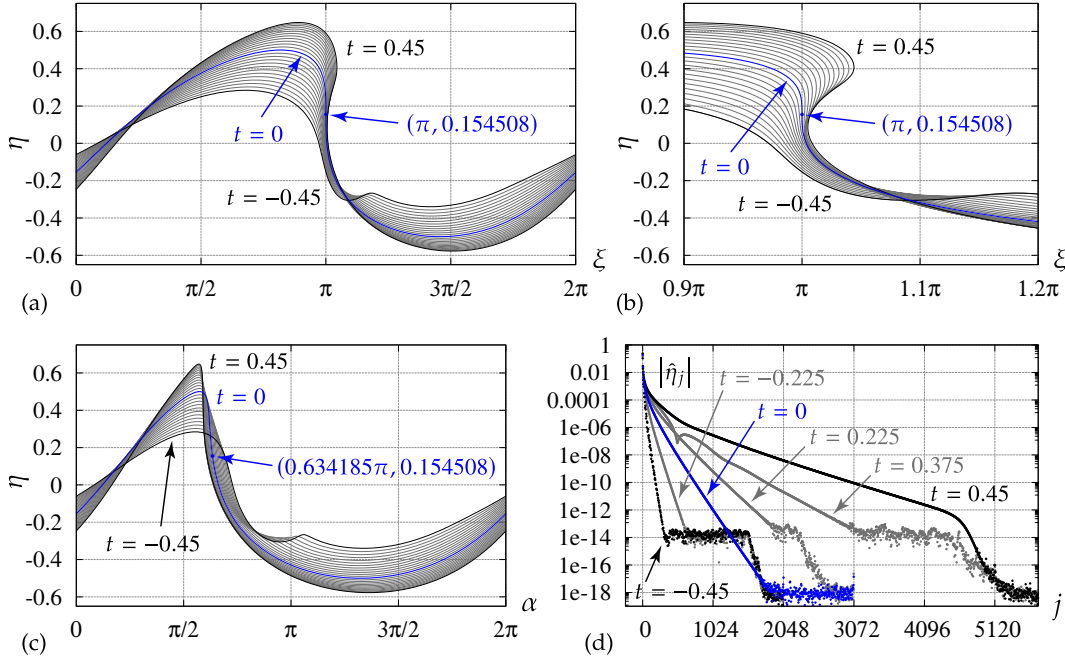


FIGURE 2. Time evolution of a spatially periodic water wave initialized via (4.2) and evolved forward and backward in time to $t = \pm 0.45$. The wave overturns for $t > 0$ and flattens out for $t < 0$. Panels (a) and (b) show snapshots of the wave in physical space; panel (c) shows snapshots of $\eta(\alpha, t)$ in conformal space; and panel (d) shows snapshots of $|\hat{\eta}_j(t)|$ in Fourier space. The initial condition ($t = 0$) is shown in blue in each plot. The blue marker denotes the vertical tangent line at $t = 0$ in panels (a) and (b) and the corresponding point in conformal space in panel (c). Note that $\eta(\alpha, t)$ remains single-valued in panel (c) but becomes very steep, causing the Fourier modes in panel (d) to decay more slowly as t increases.

and left faster than the wave crest moves down and left. Panel (f) shows the evolution of the velocity potential $\varphi(\alpha, t)$ over $0 \leq t \leq T$. Unlike $\eta_0(\alpha)$, the initial velocity potential $\varphi_0(\alpha) = \tilde{\varphi}_0(\alpha, k\alpha)$ is not 2π -periodic due to the factor of $\cos(\alpha_2 - q)$ in (4.4).

Panels (a) and (d) of Figure 4 show surface plots of $\tilde{\eta}(\alpha_1, \alpha_2, T)$ and $\tilde{\varphi}(\alpha_1, \alpha_2, T)$ at the final time computed, $T = 0.225$. The corresponding contour plots are shown in panels (b) and (c). Initially, $\tilde{\eta}(\alpha_1, \alpha_2, 0)$ depends only on α_1 ; however, by $t = T$, the dependence on α_2 is clearly visible. Although the waves overturn in some places when $\eta(\alpha, t) = \tilde{\eta}(\alpha, k\alpha, t)$ is plotted parametrically versus $\xi(\alpha, t)$ with $t > 0$ held fixed, both $\tilde{\eta}$ and $\tilde{\varphi}$ are single-valued functions of α_1 and α_2 at all times. Nevertheless, throughout the evolution, $\tilde{\eta}(\alpha_1, \alpha_2, t)$ has a steep dropoff over a narrow range of values of α_1 . Initially, $\tilde{\eta}_0(\alpha_1, \alpha_2) = \eta_2(\alpha_1) = \eta_1(\alpha_1 + B_2(\alpha_1))$ and the rapid dropoff occurs for α_1 near the solution of $\alpha_1 + B_2(\alpha_1) = \pi$ (since the vertical tangent line occurs at $\xi_1(\sigma) + i\eta_1(\sigma)$ with $\sigma = \pi$). Using Newton's method, we find that this occurs at $\alpha_1 = 0.634185\pi$. The blue curve in panel (c) of Figure 2 gives $\eta_2(\alpha)$. If one zooms in on this plot, one finds that $\eta_2(\alpha)$ decreases rapidly by more than half its crest-to-trough height over the narrow range $0.6\pi \leq \alpha \leq 0.667\pi$. At later times, $\tilde{\eta}(\alpha_1, \alpha_2, t)$ continues to drop off rapidly when α_1 traverses this narrow range in spite of the dependence on α_2 . This can be seen in panel (b) of Figure 4, where there is a high clustering of nearly vertical

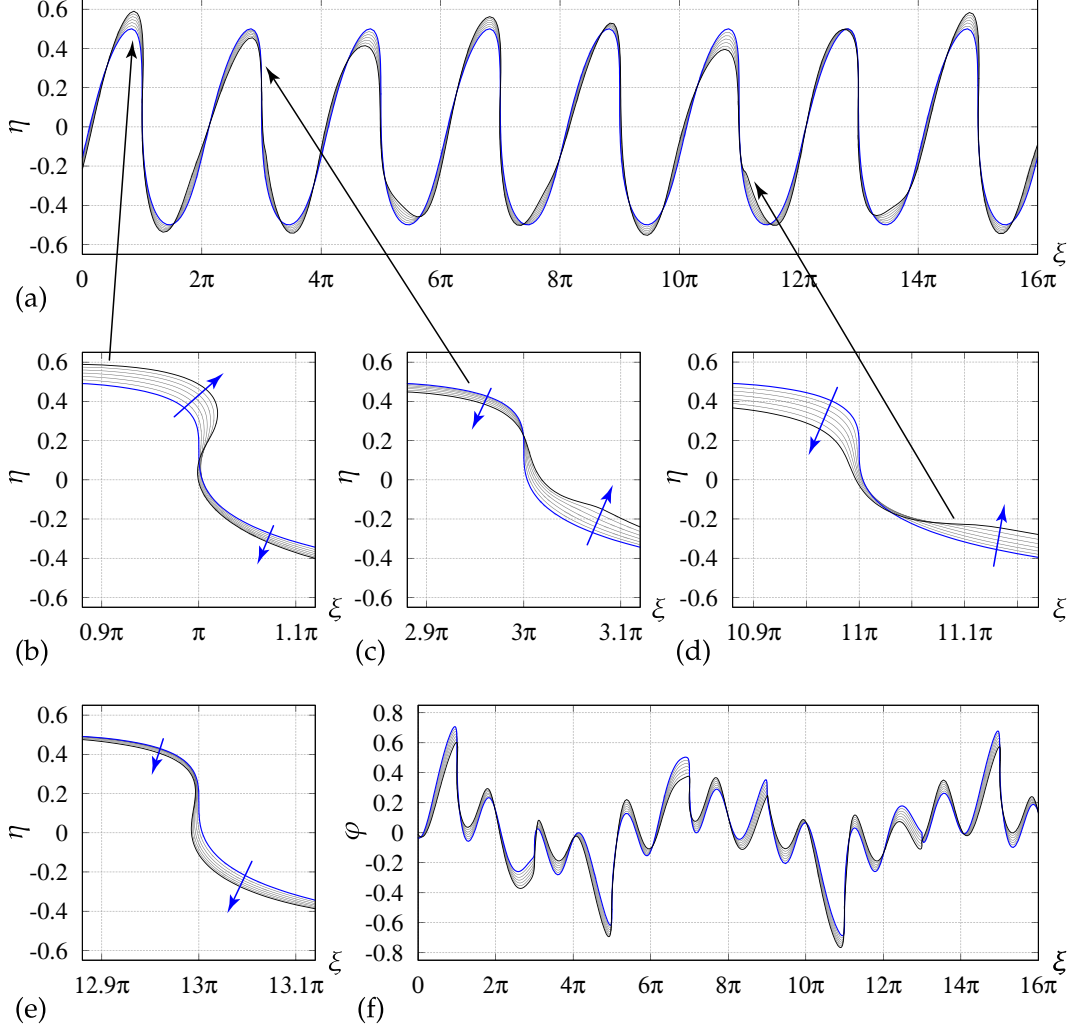


FIGURE 3. Snapshots in time of a spatially quasi-periodic water wave with a periodic initial wave profile with vertical tangent lines at $\xi = \pi + 2\pi n$, $n \in \mathbb{Z}$. A quasi-periodic initial velocity potential causes some of the waves to overturn for $t > 0$ and others to flatten out. Panels (a) and (f) show $\eta(\alpha, t)$ and $\varphi(\alpha, t)$ versus $\xi(\alpha, t)$ over $0 \leq x \leq 16\pi$ and $0 \leq t \leq T = 0.225$. Panels (b)–(e) show the results of panel (a) in more detail. The blue arrows show the direction of travel of the waves.

contour lines separating the yellow-orange region from the blue region. Over this narrow window, $\tilde{\varphi}(\alpha_1, \alpha_2, t)$ also varies rapidly with respect to α_1 .

Many gridpoints are needed to resolve these rapid variations with spectral accuracy. Although $\xi_1(\sigma)$, $\eta_1(\sigma)$ and $\varphi_1(\sigma)$ involve only a few nonzero Fourier modes, conformal reparametrization via (4.3) vastly increases the Fourier content of the initial condition. We used 6144 gridpoints to evolve the periodic auxiliary problem of Figure 2 from $t = 0$ to $t = 0.3$ and then switched to 12288 gridpoints to evolve to $t = 0.45$. Studying the Fourier modes in panel (d) of Figure 2, it appears that 4096 gridpoints (2048 modes) are sufficient to maintain double-precision accuracy forward or backward in time to $t = \pm 0.225$. Using this as a guideline for the quasi-periodic calculation, we evolved (2.40) on a 4096×4096 spatial grid using the 8th order explicit Runge-Kutta method described in Section 3. The

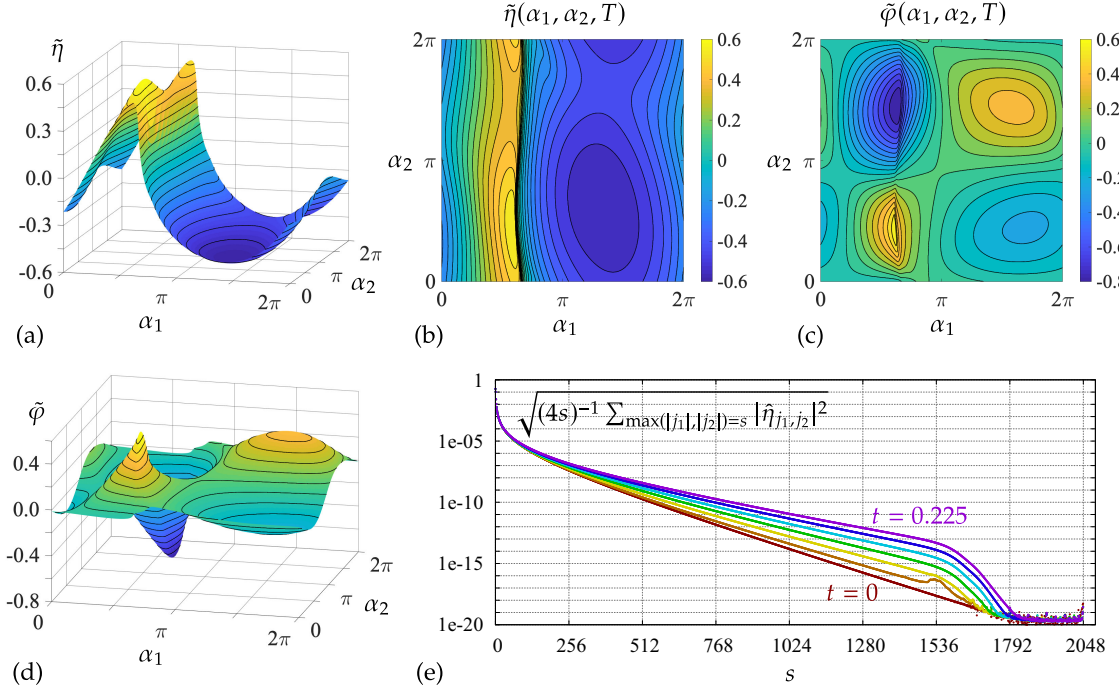


FIGURE 4. Surface and contour plots of the torus version of the solution plotted in Figure 3 at the final time $T = 0.225$. The rapid dropoff in $\tilde{\eta}(\alpha_1, \alpha_2, t)$ over the window $0.6\pi \leq \alpha_1 \leq 0.667\pi$ persists from the initial state in which $\tilde{\eta}_0(\alpha_1, \alpha_2)$ does not depend on α_2 . Panel (e) shows the exponential decay of Fourier modes with respect to the shell index s at different times.

calculation involved 5400 time steps from $t = 0$ to $t = T = 0.225$, which took 2.5 days on 12 threads running on a server with two 3.0 GHz Intel Xeon Gold 6136 processors. Additional threads had little effect on the running time as the FFT calculations require a lot of data movement relative to the number of floating point operations involved.

Panel (e) of Figure 4 shows the ℓ^2 average of the Fourier mode amplitudes $|\hat{\eta}_{j_1, j_2}|$ in each shell of indices satisfying $\max(|j_1|, |j_2|) = s$ for $1 \leq s \leq 2048$. Since $\hat{\eta}_{-j_1, -j_2} = \hat{\eta}_{j_1, j_2}$, we can discard half the modes and sweep through the lattice along straight lines from $(0, s)$ to (s, s) to $(s, -s)$ to $(1, -s)$, which sweeps out $4s$ index pairs. (The same ordering is used to enumerate the unknowns in the nonlinear least squares method proposed in [41] to compute quasi-periodic traveling water waves.) We see in panel (e) that as time increases, the modes continue to decay at an exponential rate with respect to s , but the decay rate is slower at later times. The rapid dropoff in the mode amplitudes for $s \geq 1536$ is due to the Fourier filter. At the final time $t = T = 0.225$, the modes still decay by 12 orders of magnitude from $s = 1$ to $s = 1536$, so we believe the solution is correct to 10-12 digits. A finer grid would be required to maintain this accuracy over longer times.

The rationale for setting $q = 0.6k\pi$ in (4.4) is that $\cos(\alpha_2 - q) \approx 1$ where the characteristic line $(\alpha, k\alpha)$ crosses the dropoff in the torus near $\alpha_1 = 0.6\pi$ for the first time. Locally, $\varphi_0(\alpha) = \tilde{\varphi}_0(\alpha, k\alpha)$ is close to $\varphi_3(\alpha)$, the initial condition of the auxiliary periodic problem, so we expect the quasi-periodic wave to evolve similarly to the periodic wave near $x = \pi$ for a short time. (Here $z = x + iy$ describes physical space). This is indeed what happens, which may be seen by comparing panel (b) of Figure 2 to panel (b) of Figure 3, keeping in

mind that $t \in [-0.45, 0.45]$ in the former plot and $t \in [0, 0.225]$ in the latter plot. Advancing α from 0.6π to 10.6π causes the characteristic line $(\alpha, k\alpha)$ to cross a periodic image of the dropoff at $\alpha_2 = 10.6k\pi$, where $\cos(\alpha_2 - q) = -0.9752 \approx -1$. Locally, $\varphi_0(\alpha)$ is close to $-\varphi_3(\alpha)$, the initial condition of the time-reversed auxiliary periodic problem. Thus, we expect the quasi-periodic wave to evolve similarly to the time-reversed periodic wave near $x = 11\pi$. (Recall that $\xi_0(0.634185\pi) = \pi$, so $\xi_0(10.634185\pi) = 11\pi$). Comparing panel (b) of Figure 2 to panel (d) of Figure 3 confirms that this does indeed happen. At most wave peaks, the velocity potential of the quasi-periodic solution is not closely related to that of the periodic auxiliary problem since the cosine factor is not near a relative maximum or minimum, where it is flat. As a result, the wave peaks of the quasi-periodic solution evolve in many different ways as α varies over the real line.

5. CONCLUSION

In this work, we have formulated the two-dimensional, infinite depth gravity-capillary water wave problem in a spatially quasi-periodic, conformal mapping framework. We have studied solutions of the initial value problem in which some of the wave crests overturn as time evolves while others flatten out, and have numerically verified a result in [41] that a quasi-periodic traveling wave evolves in time on the torus \mathbb{T}^2 in the direction $(1, k)$ without changing form, though the speed is non-uniform in conformal space if the condition $\tilde{\xi}(0, 0, t) = 0$ is imposed via (2.41). We developed two time-stepping strategies, an explicit Runge-Kutta approach and an exponential time differencing method, and performed a convergence study to demonstrate the effectiveness of the small-scale decomposition at removing stiffness from the evolution equations when the surface tension is large. In the appendices, we establish minimal conditions to ensure that a quasi-periodic analytic function $z(w)$ maps the lower half-plane topologically onto a region bounded above by a curve, and that $1/|z_w|$ is bounded. We also show that if all the solutions in the family are single-valued and have no vertical tangent lines, the corresponding solutions of the original graph-based formulation (2.1)–(2.4) of the Euler equations are quasi-periodic in physical space.

We believe that spatial quasi-periodicity is a natural setting to study the dynamics of linear and nonlinear waves, and has been largely overlooked as a possible third option to the usual modeling assumption that the solution either evolves on a periodic domain or decays at infinity. In the future, we plan to develop numerical methods to compute temporally quasi-periodic water waves with $n = 3$ quasi-periods, and to study subharmonic instabilities [14, 27, 29, 31, 35] of periodic traveling waves and standing waves as well as perturbations that will lead to spatially quasi-periodic dynamics.

APPENDIX A. CONFORMAL MAPPINGS OF THE LOWER HALF-PLANE

In this section we discuss sufficient conditions for an analytic function $z(w)$ to map the lower half-plane topologically onto a semi-infinite region bounded above by a parametrized curve. We will prove the following theorem, and a corollary concerning boundedness of $1/|z_w|$ when the functions are quasi-periodic.

Theorem A.1. *Suppose $\varepsilon > 0$ and $z(w)$ is analytic on the half-plane $\mathbb{C}_\varepsilon^- = \{w : \text{Im } w < \varepsilon\}$. Suppose there is a constant $M > 0$ such that $|z(w) - w| \leq M$ for $w \in \mathbb{C}_\varepsilon^-$, and that the restriction*

$\zeta = z|_{\mathbb{R}}$ is injective. Then the curve $\zeta(\alpha)$ separates the complex plane into two regions, and $z(w)$ is an analytic isomorphism of the lower half-plane onto the region below the curve $\zeta(\alpha)$.

Proof. We do not assume $\zeta(\alpha) = \xi(\alpha) + i\eta(\alpha)$ is a graph — only that it does not self-intersect. We first need to show that $\Gamma = \{\zeta(\alpha) : \alpha \in \mathbb{R}\}$ separates the complex plane into precisely two regions. (In the graph case, this is obvious.) Let $A = 2M$ and consider the linear fractional transformation

$$(A.1) \quad T(z) = -\frac{z + Ai}{z - Ai}, \quad T^{-1}(\lambda) = Ai \frac{\lambda - 1}{\lambda + 1}.$$

Note that T maps the real line to the unit circle and $T^{-1}(e^{-i\theta}) = A \tan(\theta/2)$. Let $g(\theta) = T \circ \zeta \circ T^{-1}(e^{-i\theta})$. Since $\zeta(\alpha)$ lies inside a closed ball of radius M centered at α , $\zeta(\alpha)$ remains in the strip $\text{Im } z \in [-M, M]$ and approaches complex ∞ as $\alpha \rightarrow \pm\infty$. Since $T(\infty) = -1$, g becomes continuous on $[-\pi, \pi]$ if we define $g(\pm\pi) = -1$. Since T is bijective and ζ is injective, g is a Jordan curve and separates the complex plane into two regions. The curve $g(\theta)$ takes values in the set $\{\lambda : |\lambda + 1/3| \geq 2/3, |\lambda - 1| \leq 2\}$, which is the image of the strip $\text{Im } z \in [-M, M]$ under T . An argument similar to Lemma 2 of section 4.2.1 of [1] shows that if $|\lambda + 1/3| < 2/3$, then λ is inside the Jordan curve. In particular, if $\text{Im } z < -M$, then $T(z)$ is inside the curve. We conclude that there is a well-defined “fluid” region Ω_f that is mapped topologically by T to the inside of the Jordan curve, and a “vacuum” region Ω_v that is mapped topologically to the outside of the Jordan curve.

Next we show that $z(w)$ is univalent and maps the lower half-plane onto the fluid region. Consider the path γ_a in the w -plane that traverses the boundary ∂S_a of the half-disk $S_a = \{w : |w| < a, \text{Im } w < 0\}$. Let $\Gamma = \{\zeta(\alpha) : \alpha \in \mathbb{R}\}$ and suppose $z_0 \in \Omega_f \cup \Omega_v = \mathbb{C} \setminus \Gamma$. If $a > |z_0| + M$, then $z(w) - z_0$ has no zeros on γ_a . Indeed, $w \in \gamma_a$ requires $\text{Im } w = 0$ or $|w| = a$. Assuming $z(w) = z_0$ would require $z_0 \in \Gamma$ or $|z(w)| \geq a - M > |z_0|$, a contradiction in either case. We can therefore define the winding number of $\Gamma_a = z(\gamma_a)$ around z_0 ,

$$(A.2) \quad n(\Gamma_a, z_0) = \int_{\Gamma_a} \frac{dz}{z - z_0} = \int_{\gamma_a} \frac{z'(w)dw}{z(w) - z_0}, \quad (a > |z_0| + M).$$

Since $n(\Gamma_a, z_0)$ counts the number of solutions of $z(w) = z_0$ inside S_a and all solutions in the lower half-plane belong to S_a as soon as $a > |z_0| + M$, $n(\Gamma_a, z_0)$ is a non-negative integer that gives the number of solutions of $z(w) = z_0$ in the lower half-plane. It is independent of a once $a > |z_0| + M$.

We decompose $n(\Gamma_a, z_0) = n_2(z_0, a) - n_1(z_0, a)$, where

$$(A.3) \quad n_1(z_0, a) = \frac{1}{2\pi i} \int_{-a}^a \frac{\zeta'(\alpha)d\alpha}{\zeta(\alpha) - z_0}$$

and $n_2(z_0, a)$ is given in (A.5) below. Let $n_1(z_0) = \lim_{a \rightarrow \infty} n_1(z_0, a)$. We will show that

$$(A.4) \quad n_1(z_0) = \begin{cases} -1/2, & z_0 \in \Omega_f, \\ 1/2, & z_0 \in \Omega_v. \end{cases}$$

First, if $z_0 = -iA$, where $A > M$, then $\text{Im}\{\zeta(\alpha) - z_0\} > 0$ for $\alpha \in \mathbb{R}$. Thus, $\zeta(\alpha) - z_0$ does not cross the principal branch cut of the logarithm. As a result,

$$n_1(-iA, a) = \frac{1}{2\pi i} \left[\ln \left| \frac{\zeta(a) + iA}{\zeta(-a) + iA} \right| + i \text{Arg}(\zeta(a) + iA) - i \text{Arg}(\zeta(-a) + iA) \right].$$

Since $|\zeta(\alpha) - \alpha| \leq M < A$, as $a \rightarrow \infty$ we obtain

$$n_1(-iA) = \frac{\ln(1) + i0 - i\pi}{2\pi i} = -\frac{1}{2}.$$

A similar argument shows that $n_1(iA) = 1/2$. Let $[z_0, z_1]$ denote the line segment in \mathbb{C} connecting two points z_0 and z_1 , and suppose this line segment does not intersect the curve $\zeta(\alpha)$. We claim that if the limit defining $n_1(z_0)$ exists, the limit defining $n_1(z_1)$ also exists, and $n_1(z_1) = n_1(z_0)$. First note that

$$n_1(z_1, a) = n_1(z_0, a) + \frac{1}{2\pi i} \int_{-a}^a \left[\frac{\zeta'(\alpha)}{\zeta(\alpha) - z_1} - \frac{\zeta'(\alpha)}{\zeta(\alpha) - z_0} \right] d\alpha.$$

Since $\zeta(\alpha)$ does not cross $[z_0, z_1]$, $\frac{\zeta(\alpha) - z_1}{\zeta(\alpha) - z_0}$ does not cross the negative real axis or 0. Thus,

$$n_1(z_1, a) = n_1(z_0, a) + \left[\text{Log} \frac{\zeta(\alpha) - z_1}{\zeta(\alpha) - z_0} \right]_{\alpha=-a}^{\alpha=a}.$$

Taking the limit as $a \rightarrow \infty$ gives $n_1(z_1) = n_1(z_0) + 0$, as claimed. Every point of Ω_f is connected to $-iA$ by a polygonal path that remains inside Ω_f , and every point in Ω_v is connected to iA by a polygonal path that remains inside Ω_v . The result (A.4) follows.

Next consider the contribution of the semicircular part of γ_a in (A.2), namely

$$(A.5) \quad n_2(z_0, a) = \frac{1}{2\pi i} \int_{-\pi}^0 \frac{z'(ae^{i\theta})(iae^{i\theta})}{z(ae^{i\theta}) - z_0} d\theta.$$

Since $|z(w) - w| \leq M$, the Cauchy integral formula gives $|z'(\alpha + i\beta) - 1| \leq M/(\varepsilon - \beta)$ for $\beta \in (-\infty, \varepsilon)$. For $a > 2(M + |z_0|)$,

$$|z(ae^{i\theta}) - z_0| \geq (a - M - |z_0|) > a/2,$$

thus the modulus of the integrand in (A.5) is bounded uniformly by $2(1 + M/\varepsilon)$ for large a . For fixed $\theta \in (-\pi, 0)$, $z'(ae^{i\theta}) \rightarrow 1$ and $[z(ae^{i\theta}) - z_0]/a \rightarrow e^{i\theta}$, so the integrand approaches i pointwise on the interior of the integration interval as $a \rightarrow \infty$. By the dominated convergence theorem, $\lim_{a \rightarrow \infty} n_2(z_0, a) = 1/2$. Combining these results, we find that $\lim_{a \rightarrow \infty} n(\Gamma_a, z_0) = 1/2 - n_1(z_0)$. But since $n(\Gamma_a, z_0)$ is constant for $a > |z_0| + M$, we conclude that

$$(A.6) \quad n(\Gamma_a, z_0) = \begin{cases} 1, & z_0 \in \Omega_f \\ 0, & z_0 \in \Omega_v \end{cases}, \quad (a > |z_0| + M).$$

This shows that when solving the equation $z(w) = z_0$, if $z_0 \in \Omega_f$, there is precisely one solution w_0 in the lower half-plane, and if $z_0 \in \Omega_v$, there are no solutions w_0 in the lower half-plane. Since $z(w)$ is an open mapping, it cannot map a point in the lower half-plane to the boundary Γ , since a nearby point would then have to be mapped to Ω_v . It follows that $z(w)$ is a 1-1 mapping of $\{\text{Im } w < 0\}$ onto Ω_f . It is then a standard result that $z'(w)$ has no zeros in the lower half-plane and the inverse function $w(z)$ exists and is analytic on Ω_f . \square

Example A.2. The function $z(w) = 2w^2/(2w - i)$ satisfies $|z(w) - w| = |iw|/|2w - i|$. Writing $w = \alpha + i\beta$, we have $|z(w) - w|^2 = (\alpha^2 + \beta^2)/[4\alpha^2 + (2\beta - 1)^2]$. If $\beta \in (-\infty, 1/4]$, then $(2\beta - 1)^2 = 4\beta^2 - 4\beta + 1 \geq 4\beta^2$ and $|z(w) - w|^2 \leq 1/4$. Moreover, $\zeta(\alpha) = 2\alpha^2(2\alpha + i)/(4\alpha^2 + 1)$ is injective in spite of a cusp at the origin (where $\zeta'(0) = 0$). The hypotheses of Theorem A.1 are satisfied with $\varepsilon = 1/4$ and $M = 1/2$, so z maps the half-plane \mathbb{C}^- conformally onto the

region below the curve $\zeta(\alpha)$, in spite of the cusp. We will usually assume $\zeta'(\alpha) \neq 0$ for $\alpha \in \mathbb{R}$ so that the curve is smooth.

Corollary A.3. *Suppose $k > 0$ is irrational, $\tilde{\eta}(\alpha_1, \alpha_2) = \sum_{(j_1, j_2) \in \mathbb{Z}^2} \hat{\eta}_{j_1, j_2} e^{i(j_1 \alpha_1 + j_2 \alpha_2)}$, and there exist constants C and $\varepsilon > 0$ such that*

$$(A.7) \quad \hat{\eta}_{-j_1, -j_2} = \overline{\hat{\eta}_{j_1, j_2}}, \quad |\hat{\eta}_{j_1, j_2}| \leq C e^{-3\varepsilon K \max(|j_1|, |j_2|)}, \quad (j_1, j_2) \in \mathbb{Z}^2,$$

where $K = \max(k, 1)$. Let x_0 be real and define $\tilde{\xi} = x_0 + H[\tilde{\eta}]$, $\tilde{\zeta} = \tilde{\xi} + i\tilde{\eta}$ and

$$(A.8) \quad \tilde{z}(\alpha_1, \alpha_2, \beta) = x_0 + i\hat{\eta}_{0,0} + \sum_{j_1 + j_2 k < 0} 2i\hat{\eta}_{j_1, j_2} e^{-(j_1 + j_2 k)\beta} e^{i(j_1 \alpha_1 + j_2 \alpha_2)}, \quad (\beta < \varepsilon),$$

where the sum is over all integer pairs (j_1, j_2) satisfying the inequality. Suppose also that for each fixed $\theta \in [0, 2\pi)$, the function $\alpha \mapsto \zeta(\alpha; \theta) = \alpha + \tilde{\zeta}(\alpha, \theta + k\alpha)$ is injective from \mathbb{R} to \mathbb{C} and $\zeta_\alpha(\alpha; \theta) \neq 0$ for $\alpha \in \mathbb{R}$. Then for each $\theta \in \mathbb{R}$, the curve $\zeta(\alpha; \theta)$ separates the complex plane into two regions and

$$(A.9) \quad z(\alpha + i\beta; \theta) = (\alpha + i\beta) + \tilde{z}(\alpha, \theta + k\alpha, \beta), \quad (\beta < \varepsilon)$$

is an analytic isomorphism of the lower half-plane onto the region below $\zeta(\alpha; \theta)$. Moreover, there is a constant $\delta > 0$ such that $|z_w(w; \theta)| \geq \delta$ for $\text{Im } w \leq 0$ and $\theta \in \mathbb{R}$.

Proof. First we confirm that $z(w; \theta)$ and $\zeta(w; \theta)$ satisfy the hypotheses of Theorem A.1. The formula

$$(A.10) \quad z(w; \theta) = w + x_0 + i\hat{\eta}_{0,0} + \sum_{j_1 + j_2 k < 0} (2i\hat{\eta}_{j_1, j_2} e^{ij_2 \theta}) e^{i(j_1 + j_2 k)w}$$

expresses $z(w; \theta)$ as a uniformly convergent series of analytic functions on the region $\text{Im } w < \varepsilon$, so it is analytic in this region. This follows from the inequalities

$$(A.11) \quad \begin{aligned} 0 < -(j_1 + j_2 k) &\leq |j_1| + |j_2|k \leq 2K \max(|j_1|, |j_2|), \\ -(j_1 + j_2 k)\beta &\leq -(j_1 + j_2 k)\varepsilon \leq 2\varepsilon K \max(|j_1|, |j_2|), \quad (-\infty < \beta \leq \varepsilon) \\ \left| (2i\hat{\eta}_{j_1, j_2} e^{ij_2 \theta}) e^{i(j_1 + j_2 k)w} \right| &\leq 2C e^{-\varepsilon K \max(|j_1|, |j_2|)}, \quad (\text{Im } w \leq \varepsilon) \end{aligned}$$

and the fact that for each non-negative integer s , there are $4s$ index pairs (j_1, j_2) in the shell $\max(|j_1|, |j_2|) = s$ and satisfying $j_1 + j_2 k < 0$:

$$(A.12) \quad \sum_{j_1 + j_2 k < 0} \left| (2i\hat{\eta}_{j_1, j_2} e^{ij_2 \theta}) e^{i(j_1 + j_2 k)w} \right| \leq \sum_{s=1}^{\infty} (2C)(4s) e^{-\varepsilon K s} < \infty, \quad (\text{Im } w \leq \varepsilon).$$

This also implies that there is a bound M such that $|z(w; \theta) - w| \leq M$ for $\text{Im } w \leq \varepsilon$ and $\theta \in \mathbb{R}$. Let $\xi(\alpha; \theta) = \alpha + \tilde{\xi}(\alpha, \theta + k\alpha)$ and $\eta(\alpha; \theta) = \tilde{\eta}(\alpha, \theta + k\alpha)$ denote the real and imaginary parts of $\zeta(\alpha; \theta)$. Setting $w = \alpha \in \mathbb{R}$ in (A.10) and taking real and imaginary parts confirms that $z(w; \theta)|_{w=\alpha} = \zeta(\alpha; \theta)$. By assumption, $\zeta(\alpha; \theta)$ is injective, so Theorem A.1 implies that $z(w; \theta)$ is an analytic isomorphism of the lower half-plane onto the region below the curve $\zeta(\alpha; \theta)$. Differentiating (A.10) term by term [1] shows that $z_w(\alpha + i\beta; \theta) = F(\alpha, \theta + k\alpha, \beta)$, where

$$(A.13) \quad F(\alpha_1, \alpha_2, \beta) = 1 - \sum_{j_1 + j_2 k < 0} 2(j_1 + j_2 k) \hat{\eta}_{j_1, j_2} e^{-(j_1 + j_2 k)\beta} e^{i(j_1 \alpha_1 + j_2 \alpha_2)}.$$

We claim that $F(\alpha_1, \alpha_2, \beta) \rightarrow 1$ uniformly in (α_1, α_2) as $\beta \rightarrow -\infty$. Indeed, arguing as in (2.23), we see that $|F(\alpha_1, \alpha_2, \beta) - 1| = |z_w(\alpha_1 + i\beta; \alpha_2 - k\alpha_1) - 1| \leq M/(\varepsilon - \beta)$. Thus,

for $\beta \leq -B$ with $B = 2M$, $|F(\alpha_1, \alpha_2, \beta)| \geq 1/2$. Since $|F(\alpha_1, \alpha_2, \beta)|$ is continuous, it achieves its minimum over $(\alpha_1, \alpha_2) \in \mathbb{T}^2$ and $-B \leq \beta \leq 0$. Denote this minimum by δ . If δ were zero, there would exist α_1, α_2 and $\beta \leq 0$ such that $F(\alpha_1, \alpha_2, \beta) = 0$. But then $z_w(\alpha_1 + i\beta; \theta) = F(\alpha_1, \theta + k\alpha_1, \beta) = 0$ with $\theta = \alpha_2 - k\alpha_1$. The case $\beta = 0$ is ruled out by the assumption that $\zeta_\alpha(\alpha; \theta) \neq 0$ while $\beta < 0$ contradicts $z(w; \theta)$ being 1-1 on \mathbb{C}^- . So $\delta > 0$ and $|F(\alpha_1, \alpha_2, \beta)| \geq \min(\delta, 1/2)$ for all $\beta \leq 0$. Decreasing δ to $1/2$ if necessary gives the desired lower bound $|z_w(w; \theta)| \geq \delta$. \square

APPENDIX B. QUASI-PERIODIC FAMILIES OF SOLUTIONS

In this appendix we explore the effect of introducing phases in the reconstruction of one-dimensional quasi-periodic solutions of (2.40) from solutions of the torus version of these equations. This ultimately makes it possible to show that if all the solutions in the family are single-valued and have no vertical tangent lines, the corresponding solutions of the original graph-based formulation (2.1)–(2.4) of the Euler equations are quasi-periodic in physical space.

Theorem B.1. *The solution pair $(\tilde{\zeta}, \tilde{\varphi})$ on the torus represents an infinite family of quasi-periodic solutions on \mathbb{R} given by*

$$(B.1) \quad \begin{aligned} \zeta(\alpha, t; \theta_1, \theta_2, \delta) &= \alpha + \delta + \tilde{\zeta}(\theta_1 + \alpha, \theta_2 + k\alpha, t), \\ \varphi(\alpha, t; \theta_1, \theta_2) &= \tilde{\varphi}(\theta_1 + \alpha, \theta_2 + k\alpha, t), \end{aligned} \quad \left(\begin{array}{l} \alpha \in \mathbb{R}, t \geq 0 \\ \theta_1, \theta_2, \delta \in \mathbb{R} \end{array} \right).$$

Proof. We claim that by solving (2.40) throughout \mathbb{T}^2 in the sense of Remark 2.3, any one-dimensional (1d) slice of the form (B.1) will satisfy the kinematic condition (2.33) and the Bernoulli equation (2.39). Let us freeze θ_1, θ_2 and δ and drop them from the notation on the left-hand side of (B.1). Consider substituting $\eta = \text{Im } \zeta$ and φ from (B.1) into (2.40), and let $u(\alpha) = \tilde{u}(\theta_1 + \alpha, \theta_2 + k\alpha)$ represent the input of any α -derivative or Hilbert transform in an intermediate calculation. Both η and φ are of this form. By Remark 2.2, $H[u](\alpha) = H[\tilde{u}](\theta_1 + \alpha, \theta_2 + k\alpha)$, and clearly $u'(\alpha) = [(\partial_{\alpha_1} + k\partial_{\alpha_2})\tilde{u}](\theta_1 + \alpha, \theta_2 + k\alpha)$, so the output retains this form. We conclude that computing (2.40) on the torus gives the same results for $\tilde{\eta}_t$ and $\tilde{\varphi}_t$ when evaluated at $(\theta_1 + \alpha, \theta_2 + k\alpha)$ as the 1d calculations of η_t and φ_t when evaluated at α . Since $\tilde{\xi}(\cdot, t) = x_0(t) + H[\tilde{\eta}(\cdot, t)]$ on \mathbb{T}^2 ,

$$(B.2) \quad \xi(\alpha, t) = \alpha + \delta + x_0(t) + H[\eta(\cdot, t)](\alpha),$$

which follows from (B.1) and $H[\eta(\cdot, t)](\alpha) = H[\tilde{\eta}(\cdot, t)](\theta_1 + \alpha, \theta_2 + k\alpha)$. Thus, computing $\xi_\alpha = 1 + H[\eta_\alpha]$ in (2.40) gives the same result as just differentiating ξ from (B.1) and (B.2). In the 1d problem, the right-hand side of (2.36) represents complex multiplication of z_α with a bounded analytic function (namely z_t/z_α) whose imaginary part equals $-\chi$ on the real axis; thus, in (2.36), ξ_t differs from $H[\eta_t]$ by a constant. This constant is determined by comparing ξ_t in (2.36) with ξ_t from (B.2), which leads to the same formula (2.37) for dx_0/dt that is used in the torus calculation. Here we note that a phase shift does not affect the mean of a periodic function on the torus, i.e. $P_0[S_\theta \tilde{u}] = P_0[\tilde{u}]$ where $S_\theta[\tilde{u}](\alpha) = \tilde{u}(\alpha + \theta)$. We have assumed that in the 1d calculation, C_1 is chosen to agree with that of the torus calculation. Since C_1 only affects the tangential velocity of the interface parametrization, it can be specified arbitrarily. Left-multiplying (2.36) by $(-\eta_\alpha, \xi_\alpha)$ eliminates C_1 and yields the kinematic condition (2.33). Since the Bernoulli equation (2.39) holds on the torus, it also holds in the 1d calculation, as claimed. \square

For each solution in the family (B.1), there are many others that represent identical dynamics up to a spatial phase shift or α -reparametrization. Changing δ merely shifts the solution in physical space. In fact, δ does not appear in the equations of motion (2.36) — it is only used to reconstruct the curve via (B.2). The relations

$$(B.3) \quad \begin{aligned} \zeta(\alpha + \alpha_0, t; \theta_1, \theta_2, \delta) &= \zeta(\alpha, t; \theta_1 + \alpha_0, \theta_2 + k\alpha_0, \delta + \alpha_0), \\ \varphi(\alpha + \alpha_0, t; \theta_1, \theta_2) &= \varphi(\alpha, t; \theta_1 + \alpha_0, \theta_2 + k\alpha_0), \end{aligned}$$

show that shifting α by α_0 leads to another solution already in the family. This shift reparametrizes the curve but has no effect on its evolution in physical space. If we identify two solutions that differ only by a spatial phase shift or α -reparametrization, the parameters $(\theta_1, \theta_2, \delta)$ become identified with $(0, \theta_2 - k\theta_1, 0)$. Every solution is therefore equivalent to one of the form

$$(B.4) \quad \begin{aligned} \zeta(\alpha, t; 0, \theta, 0) &= \alpha + \tilde{\zeta}(\alpha, \theta + k\alpha, t), \\ \varphi(\alpha, t; 0, \theta) &= \tilde{\varphi}(\alpha, \theta + k\alpha, t) \end{aligned} \quad \alpha \in \mathbb{R}, \quad t \geq 0, \quad \theta \in [0, 2\pi).$$

Within this smaller family, two values of θ lead to equivalent solutions if they differ by $2\pi(n_1k + n_2)$ for some integers n_1 and n_2 . This equivalence is due to solutions “wrapping around” the torus with a spatial shift,

$$(B.5) \quad \zeta(\alpha + 2\pi n_1, t; 0, \theta, 0) = \zeta(\alpha, t; 0, \theta + 2\pi(n_1k + n_2), 2\pi n_1), \quad (\alpha \in [0, 2\pi), \quad n_1 \in \mathbb{Z}).$$

Here n_2 is chosen so that $0 \leq [\theta + 2\pi(n_1k + n_2)] < 2\pi$ and we used periodicity of $\zeta(\alpha, t; \theta_1, \theta_2, \delta)$ with respect to θ_1 and θ_2 . It usually suffices to restrict attention to $\alpha \in [0, 2\pi)$ by making use of (B.5). One exception is determining whether the curve self-intersects. In that case it is more natural to tile the plane with periodic copies of the torus and consider the straight line parametrization of (B.4). Indeed, it is conceivable that

$$(B.6) \quad \zeta(\alpha, t; 0, \theta, 0) = \zeta(\beta, t; 0, \theta, 0)$$

with $|\alpha - \beta|$ as large as $2M$, where M is a bound on $|\tilde{\zeta}|$ over \mathbb{T}^2 , and the condition (B.6) becomes hard to understand if (B.5) is used to map α and β back to $[0, 2\pi)$ with different choices of n_1 or n_2 .

The following theorem shows that $\eta^{\text{phys}}(x, t; \theta_1, \theta_2, \delta)$ and $\varphi^{\text{phys}}(x, t; \theta_1, \theta_2, \delta)$ can be computed easily from $\zeta(\alpha, t; \theta_1, \theta_2, \delta)$ and $\varphi(\alpha, t; \theta_1, \theta_2)$ if all of the waves in the family (B.4) are single-valued and have no vertical tangent lines, and that η^{phys} and φ^{phys} are quasi-periodic functions of x .

Theorem B.2. *Fix $t \geq 0$ and suppose $\xi_\alpha(\alpha, t; 0, \theta, 0) > 0$ for all $(\alpha, \theta) \in [0, 2\pi) \times [0, 2\pi)$. Then there is a periodic, real analytic function $\mathcal{A}(x_1, x_2, t)$ defined on \mathbb{T}^2 satisfying*

$$(B.7) \quad \mathcal{A}(x_1, x_2, t) + \tilde{\xi}(x_1 + \mathcal{A}(x_1, x_2, t), x_2 + k\mathcal{A}(x_1, x_2, t), t) = 0, \quad (x_1, x_2) \in \mathbb{T}^2.$$

Given $\theta \in [0, 2\pi)$, the change of variables $\alpha = x + \mathcal{A}(x, \theta + kx, t)$ satisfies

$$(B.8) \quad \xi(\alpha, t; 0, \theta, 0) = \alpha + \tilde{\xi}(\alpha, \theta + k\alpha, t) = x, \quad (x \in \mathbb{R}).$$

This allows us to express solutions in the family (B.4) as functions of x and t ,

$$(B.9) \quad \begin{aligned} \eta^{\text{phys}}(x, t; 0, \theta, 0) &= \eta(\alpha, t; 0, \theta, 0), \\ \varphi^{\text{phys}}(x, t; 0, \theta, 0) &= \varphi(\alpha, t; 0, \theta), \end{aligned} \quad \left(\alpha = x + \mathcal{A}(x, \theta + kx, t) \right).$$

These functions are real analytic, quasi-periodic functions of x in the sense that

$$(B.10) \quad \begin{aligned} \eta^{\text{phys}}(x, t; 0, \theta, 0) &= \tilde{\eta}^{\text{phys}}(x, \theta + kx, t) \\ \varphi^{\text{phys}}(x, t; 0, \theta, 0) &= \tilde{\varphi}^{\text{phys}}(x, \theta + kx, t) \end{aligned}$$

with

$$(B.11) \quad \begin{aligned} \tilde{\eta}^{\text{phys}}(x_1, x_2, t) &= \tilde{\eta}(x_1 + \mathcal{A}(x_1, x_2, t), x_2 + k\mathcal{A}(x_1, x_2, t), t), \\ \tilde{\varphi}^{\text{phys}}(x_1, x_2, t) &= \tilde{\varphi}(x_1 + \mathcal{A}(x_1, x_2, t), x_2 + k\mathcal{A}(x_1, x_2, t), t). \end{aligned}$$

More generally, one can define

$$(B.12) \quad \begin{aligned} \eta^{\text{phys}}(x, t; \theta_1, \theta_2, \delta) &= \eta(\alpha, t; \theta_1, \theta_2, \delta) = \tilde{\eta}^{\text{phys}}(\theta_1 + x - \delta, \theta_2 + k(x - \delta), t) \\ \varphi^{\text{phys}}(x, t; \theta_1, \theta_2, \delta) &= \varphi(\alpha, t; \theta_1, \theta_2) = \tilde{\varphi}^{\text{phys}}(\theta_1 + x - \delta, \theta_2 + k(x - \delta), t) \end{aligned}$$

with $\alpha = x - \delta + \mathcal{A}(\theta_1 + x - \delta, \theta_2 + k(x - \delta), t)$ to express $\zeta(\alpha, t; \theta_1, \theta_2, \delta)$ as a graph and $\varphi(\alpha, t; \theta_1, \theta_2)$ as a function of x .

Proof. From (B.1), we know that $\xi_\alpha(\alpha, t; 0, \theta, 0)$ is 2π -periodic in θ . Thus, it is positive for $\alpha \in [0, 2\pi)$ and $\theta \in \mathbb{R}$. Since $1 + [\partial_{\alpha_1} + k\partial_{\alpha_2}] \tilde{\xi}(\alpha_1, \alpha_2, t) = \xi_\alpha(\alpha_1, t; 0, \alpha_2 - k\alpha_1, 0)$ is positive, periodic and continuous for $(\alpha_1, \alpha_2) \in \mathbb{T}^2$, it is bounded below by a positive constant $\varepsilon > 0$. Let $M(t)$ be a bound on $|\tilde{\xi}(\alpha_1, \alpha_2, t)|$ over \mathbb{T}^2 . Then for fixed $(x_1, x_2) \in \mathbb{R}^2$, the function $g(\alpha) = g(\alpha; x_1, x_2) = \alpha + \tilde{\xi}(x_1 + \alpha, x_2 + k\alpha, t)$ is strictly monotonically increasing (as $g'(\alpha) \geq \varepsilon$) and satisfies $g(-M) \leq 0$ and $g(M) \geq 0$. Thus, we can define $\mathcal{A}(x_1, x_2, t)$ as the unique solution of $g(\alpha) = 0$, and $|\mathcal{A}(x_1, x_2, t)| \leq M$. If n_1 and n_2 are integers and $y_1 = x_1 + 2\pi n_1$ and $y_2 = x_2 + 2\pi n_2$, then $\alpha = \mathcal{A}(x_1, x_2)$ satisfies $\alpha + \tilde{\xi}(y_1 + \alpha, y_2 + k\alpha, t) = 0$, so $\mathcal{A}(y_1, y_2, t) = \mathcal{A}(x_1, x_2, t)$. This shows that $\mathcal{A}(x_1, x_2, t)$ is periodic in (x_1, x_2) , and hence well-defined on \mathbb{T}^2 . It is also real analytic, which follows from the implicit function theorem, noting that $g(\alpha; x_1, x_2)$ is real analytic in all three variables and $\partial g / \partial \alpha$ is never zero.

The first equality of (B.8) is the definition of $\xi(\alpha, t; 0, \theta, 0)$ and the second follows from (B.7) when $\alpha = x + \mathcal{A}(x, \theta + kx, t)$ is substituted into $\alpha + \tilde{\xi}(\alpha, \theta + k\alpha, t)$. From (B.9) and (B.4) we have

$$(B.13) \quad \begin{aligned} \eta^{\text{phys}}(x, t; 0, \theta, 0) &= \tilde{\eta}(\alpha, \theta + k\alpha, t), \\ \varphi^{\text{phys}}(x, t; 0, \theta, 0) &= \tilde{\varphi}(\alpha, \theta + k\alpha, t), \end{aligned}$$

where $\alpha = x + \mathcal{A}(x, \theta + kx, t)$. Comparing (B.13) with (B.11) gives (B.10). Equation (B.12) is derived similarly using (B.1), (B.7) and (B.11) to check that

$$(B.14) \quad \begin{aligned} \xi(\alpha, t; \theta_1, \theta_2, \delta) &= \alpha, \\ \eta(\alpha, t; \theta_1, \theta_2, \delta) &= \tilde{\eta}^{\text{phys}}(\theta_1 + x - \delta, \theta_2 + k(x - \delta), t), \\ \varphi(\alpha, t; \theta_1, \theta_2) &= \tilde{\varphi}^{\text{phys}}(\theta_1 + x - \delta, \theta_2 + k(x - \delta), t) \end{aligned}$$

when $\alpha = x - \delta + \mathcal{A}(\theta_1 + x - \delta, \theta_2 + k(x - \delta), t)$. \square

REFERENCES

- [1] Lars Ahlfors. *Complex Analysis*. McGraw-Hill, New York, 1979.
- [2] Benjamin F Akers and Wenxuan Gao. Wilton ripples in weakly nonlinear model equations. *Communications in Mathematical Sciences*, 10(3):1015–1024, 2012.
- [3] D. M. Ambrose, R. Camassa, J. L. Marzuola, R. McLaughlin, Q. Robinson, and J. Wilkening. Numerical algorithms for water waves with background flow over obstacles and topography. 2020. (in preparation).

- [4] Sheldon Axler, Paul Bourdon, and Wade Ramey. *Harmonic Function Theory*. Springer-Verlag, New York, 1992.
- [5] Pietro Baldi, Massimiliano Berti, Emanuele Haus, and Riccardo Montalto. Time quasi-periodic gravity water waves in finite depth. *Inventiones mathematicae*, 214(2):739–911, 2018.
- [6] J.-P. Berenger. A perfectly matched layer for the absorption of electromagnetic waves. *J. Comput. Phys.*, 114:185–200, 1994.
- [7] H. Berland, B. Owren, and B. Skaflestad. B-series and order conditions for exponential integrators. *SIAM J. Numer. Anal.*, 43(4):1715–1727, 2005.
- [8] Massimiliano Berti and Riccardo Montalto. Quasi-periodic standing wave solutions of gravity-capillary water waves. *arXiv preprint arXiv:1602.02411*, 2016.
- [9] TJ Bridges and F Dias. Spatially quasi-periodic capillary-gravity waves. *Contemporary Mathematics*, 200:31–46, 1996.
- [10] J. Chen and J. Wilkening. Arbitrary-order exponential time differencing schemes via Chebyshev moments of exponential functions. 2020. (in preparation).
- [11] Wooyoung Choi and Roberto Camassa. Exact evolution equations for surface waves. *Journal of engineering mechanics*, 125(7):756–760, 1999.
- [12] S.M. Cox and P.C. Matthews. Exponential time differencing for stiff systems. *J. Comput. Phys.*, 176(2):430–455, 2002.
- [13] W. Craig and C. Sulem. Numerical simulation of gravity waves. *J. Comp. Phys.*, 108:73–83, 1993.
- [14] B. Deconinck and K. Oliveras. The instability of periodic surface gravity waves. *J. Fluid Mech.*, 675:141–167, 2011.
- [15] S. Yu. Dobrokhotov and I. M. Krichever. Multi-phase solutions of the Benjamin-Ono equation and their averaging. *Math. Notes*, 49:583–594, 1991.
- [16] Alexander I Dyachenko, Evgenii A Kuznetsov, MD Spector, and Vladimir E Zakharov. Analytical description of the free surface dynamics of an ideal fluid (canonical formalism and conformal mapping). *Physics Letters A*, 221(1-2):73–79, 1996.
- [17] Alexander I Dyachenko, Vladimir E Zakharov, and Evgenii A Kuznetsov. Nonlinear dynamics of the free surface of an ideal fluid. *Plasma Physics Reports*, 22(10):829–840, 1996.
- [18] Sergey A Dyachenko, Pavel M Lushnikov, and Alexander O Korotkevich. Branch cuts of stokes wave on deep water. Part I: Numerical solution and Padé approximation. *Studies in Applied Mathematics*, 137(4):419–472, 2016.
- [19] H. Flaschka, M. G. Forest, and D. W. McLaughlin. Multiphase averaging and the inverse spectral solution of the Korteweg-de Vries equation. *Comm. Pure Appl. Math.*, 33:739–784, 1980.
- [20] Ernst Hairer, Syvert P. Norsett, and Gerhard Wanner. *Solving Ordinary Differential Equations I: Nonstiff Problems*. Springer, Berlin, 2nd edition, 2000.
- [21] T. Y. Hou and R. Li. Computing nearly singular solutions using pseudo-spectral methods. *J. Comput. Phys.*, 226:379–397, 2007.
- [22] T. Y. Hou, J. S. Lowengrub, and M. J. Shelley. Removing the stiffness from interfacial flows with surface tension. *J. Comput. Phys.*, 114:312–338, 1994.
- [23] T. Y. Hou, J. S. Lowengrub, and M. J. Shelley. Boundary integral methods for multicomponent fluids and multiphase materials. *J. Comput. Phys.*, 169:302–362, 2001.
- [24] Aly-Khan Kassam and Lloyd N. Trefethen. Fourth-order time-stepping for stiff PDEs. *SIAM J. Sci. Comput.*, 26(4):1214–1233, 2005.
- [25] P. Lax. Almost periodic solutions of the KdV equation. *SIAM Review*, 18(3):351–375, 1976.
- [26] Yi A Li, James M Hyman, and Wooyoung Choi. A numerical study of the exact evolution equations for surface waves in water of finite depth. *Studies in applied mathematics*, 113(3):303–324, 2004.
- [27] M. S. Longuet-Higgins. The instabilities of gravity waves of finite amplitude in deep water. II. Subharmonics. *Proc. R. Soc. Lond. A*, 360:489–505, 1978.
- [28] M. S. Longuet-Higgins and M. J. H. Fox. Theory of the almost-highest wave. Part 2. Matching and analytic extension. *J. Fluid Mech.*, 85(4):769–786, 1978.
- [29] R. S. MacKay and P. G. Saffman. Stability of water waves. *Proc. R. Soc. Lond. A*, 406:115–125, 1986.
- [30] Daniel I Meiron, Steven A Orszag, and Moshe Israeli. Applications of numerical conformal mapping. *Journal of Computational Physics*, 40(2):345–360, 1981.

- [31] G N Mercer and A J Roberts. Standing waves in deep water: Their stability and extreme form. *Phys. Fluids A*, 4(2):259–269, 1992.
- [32] W G Penney and A T Price. Finite periodic stationary gravity waves in a perfect liquid, part II. *Phil. Trans. R. Soc. London A*, 244:254–284, 1952.
- [33] J. W. S. Rayleigh. Deep water waves, progressive or stationary, to the third order approximation. *Proc. R. Soc. A*, 91:345–353, 1915.
- [34] G. G. Stokes. On the theory of oscillatory waves. *Trans. Camb. Philos. Soc.*, 8:441–455, 1847.
- [35] O. Trichtchenko, B. Deconinck, and J. Wilkening. The instability of Wilton’s ripples. *Wave Motion*, 66:147–155, 2016.
- [36] Jean-Marc Vanden-Broeck. *Gravity–Capillary Free–Surface Flows*. Cambridge University Press, Cambridge, 2010.
- [37] P. Whalen, M. Brio, and J.V. Moloney. Exponential time-differencing with embedded Runge–Kutta adaptive step control. *J. Comput. Phys.*, 280:579–601, 2015.
- [38] J. Wilkening. Breakdown of self-similarity at the crests of large amplitude standing water waves. *Phys. Rev. Lett*, 107:184501, 2011.
- [39] J. Wilkening. Relative-periodic elastic collisions of water waves. *Contemp. Math.*, 635:109–129, 2015.
- [40] J. Wilkening. Traveling-standing water waves and their stability. 2020. (in preparation).
- [41] J. Wilkening and X. Zhao. Quasi-periodic traveling gravity-capillary waves. 2020. (submitted).
- [42] JR Wilton. On ripples. *The London, Edinburgh, and Dublin Philosophical Magazine and Journal of Science*, 29(173):688–700, 1915.
- [43] V. E. Zakharov. Stability of periodic waves of finite amplitude on the surface of a deep fluid. *Zhurnal Prikladnoi Mekhaniki i Tekhnicheskoi Fiziki*, 8:86–94, 1968.
- [44] Vladimir E Zakharov, Alexander I Dyachenko, and Oleg A Vasilyev. New method for numerical simulation of a nonstationary potential flow of incompressible fluid with a free surface. *European Journal of Mechanics-B/Fluids*, 21(3):283–291, 2002.

DEPARTMENT OF MATHEMATICS, UNIVERSITY OF CALIFORNIA AT BERKELEY, BERKELEY, CA, 94720, USA

E-mail address: wilkening@berkeley.edu

E-mail address: zhaoxinyu@berkeley.edu